

**MARMARA UNIVERSITY
INSTITUTE FOR GRADUATE STUDIES
IN PURE AND APPLIED SCIENCES**



**DESIGN OF A SENSORLESS BLDC MOTOR
DRIVER USING FIELD ORIENTED
CONTROL FOR A WASHING MACHINE**

FATİH BAYIR

MASTER THESIS

Department of Electrical and Electronics Engineering

Thesis Supervisor

Doç. Dr. Mustafa ONAT

ISTANBUL, 2019



MARMARA UNIVERSITY
INSTITUTE FOR GRADUATE STUDIES
IN PURE AND APPLIED SCIENCES



DESIGN OF A SENSORLESS BLDC MOTOR DRIVER USING FIELD ORIENTED CONTROL FOR A WASHING MACHINE

FATİH BAYIR
(525015018)

MASTER THESIS

Department of Electrical and Electronics Engineering

Thesis Supervisor

Doç. Dr. Mustafa ONAT

ISTANBUL, 2019

MARMARA UNIVERSITY
INSTITUTE FOR GRADUATE STUDIES
IN PURE AND APPLIED SCIENCES

Fatih BAYIR, a Master of Science student of Marmara University Institute for Graduate Studies in Pure and Applied Sciences, defended his thesis entitled “**Design of a Sensorless BLDC Motor Driver Using Field Oriented Control for a Washing Machine**”, on 02.12.2019 and has been found to be satisfactory by the jury members.

Jury Members

Doç.Dr. Mustafa ONAT

(Advisor)

Marmara University (SIGN)

Prof.Dr. Murat DOĞRUEL

(Jury Member)

Marmara University (SIGN)

Dr.Öğr.Üyesi Haydar BAYAR


(Jury Member)

Yıldız Teknik University (SIGN)

APPROVAL

Marmara University Institute for Graduate Studies in Pure and Applied Sciences Executive Committee approves that Fatih BAYIR be granted the degree of Master of Science in Department of Electrical and Electronics Engineering, Electrical and Electronics Engineering Program, on 02.01.2020. (Resolution no: 2020/01-02).

Director of the Institute
Prof. Dr. Bülent EKİCİ



ACKNOWLEDGMENT

Firstly, all praise is to God Almighty, the creator of everything. I would like to thank my thesis advisor for his valuable guidance and supervising. During this thesis study, he always taught me how to improve and use engineering and academic skills. His comments and suggestions were really wise. I also want to thank my wife who has supported me with no hesitation in any circumstance. Her sacrifice is deserved to be mentioned here. Besides, I must thank all my teachers who had affected me in a good manner during my whole education life. Furthermore, I would like to thank BAPKO (Bilimsel Arařtırma Projeleri Birimi) for their support through Project Number: FEN-C-YLP-090518-0257

Fatih BAYIR

Istanbul, November 2019

TABLE OF CONTENTS

ACKNOWLEDGMENT	i
TABLE OF CONTENTS	ii
ABSTRACT	iv
ÖZET	v
SYMBOLS.....	vi
ABBREVIATIONS	vii
LIST OF FIGURES.....	viii
LIST OF TABLES.....	x
1. INTRODUCTION	1
2. WASHING MACHINE.....	3
2.1. Operation Cycles in a Washing Machine	3
2.1.1. Washing cycle	4
2.1.2. Rinsing cycle	4
2.1.3. Distributing cycle	5
2.1.4. Spinning-drying cycle	5
3. PERMANENT MAGNET MOTORS.....	6
3.1. Basic Structure.....	6
3.2. Differences Between BLDC and PMSM	8
4. PMSM MODELING.....	10
4.1. Electrical Equivalent of PMSM.....	11
4.2. Stationary ($\alpha\beta$) Reference Frame	13
4.3. dq Rotating Reference Frame	16
4.4. Mechanical Dynamics of PMSM	19
5. INVERTERS AND MODULATION TECHNIQUES	21
5.1. Inverters	21
5.1.1. Current source inverters	21
5.1.2. Voltage source inverters	22
5.2. Modulation Techniques for Gating Signals.....	23
5.2.1. Sinusoidal Pulse Width Modulation.....	24
5.2.2. Space Vector Pulse Width Modulation	24
5.2.3. SVPWM technique	28
6. PMSM DRIVE WITH SENSORLESS CONTROL	34

6.1. FOC Scheme.....	34
6.2. Position Detection Methods in FOC.....	36
6.2.1. Sensored Method	37
6.2.2 Sensorless Method.....	37
6.3. Position Estimator Based on Sliding Mode Current Observer	39
6.4. Speed and Current Control Loops	41
6.4.1. PI controller	42
6.4.2. Power function based controller (PBC).....	43
7. SIMULATION STUDY.....	46
8. EXPERIMENTAL RESULTS	56
9. CONCLUSION	66
REFERENCES	67
APPENDIX A.....	71
APPENDIX B.....	72
APPENDIX C.....	73
RESUME	75

ABSTRACT

DESIGN OF A SENSORLESS BLDC MOTOR DRIVER USING FIELD ORIENTED CONTROL FOR A WASHING MACHINE

Brushless Motors (BLM) are one of the opportunities offered by the rapidly developing electric motor technology. They have been widely used in recent years since they have many advantages such as smaller size, higher speed and higher efficiency compared to brushed motors. However, the increasing usage of brushless motors in the industry has led to the necessity of designing efficient drivers for such motors. In this thesis, a driver design for a brushless motor used in washing machines is realized. In this study, the driver design is conducted in two main stages: system modeling and obtaining simulation results; experimental study for driver design.

The best known method to obtain high efficiency from brushless motors is to use the Field Oriented Control algorithm. In the Field Oriented Control, the sinusoidal signals generated by the Voltage Source Inverter (VSI) are converted to direct current quantities using some complex mathematical transformations. As it is more appropriate to apply any controller (e.g. PI controller) to the systems whose reference input and feedback input are not frequency dependent. In this thesis, a new control technique, the Power Function Based Control (PBC), is also applied to the system to obtain the results in compared to PI controllers, which is the common technique used for speed and torque control in the Field Oriented Control algorithm.

Since the Field Oriented Control (FOC) is an algorithm that operates with intensive mathematical transformations, it could be only possible to execute this kind of algorithm in real-time, by a high-performance digital signal processor (DSP) based microcontrollers. In the experimental study part of the thesis, a powerful DSP named TMS320F28035 which is a member of Texas Instrument C2000 microcontroller family is used. The experimental setup is also based on the HVDMC kit of Texas Instruments.

The modeling and simulation studies are performed in MATLAB / Simulink environment.

ÖZET

ÇAMAŞIR MAKİNESİ İÇİN ALAN YÖNLENDİRMELİ KONTROL KULLANILARAK SENSÖRSÜZ FIRÇASIZ DOĞRU AKIM MOTORU (FDAM) SÜRÜCÜSÜ TASARIMI

Fırçasız motorlar (FM), hızla gelişen elektrik motoru teknolojisinin sunduğu imkanlardan biridir. Fırçalı motorlara kıyasla, daha küçük boyut, daha yüksek hız, daha yüksek verim gibi bir çok avantajı olduğu için son yıllarda yaygın biçimde kullanılmaya başlanmışlardır. Bununla birlikte, endüstride fırçasız motorların kullanımının artması bu tip motorlar için verimli sürücü tasarımının gerekliliğini doğurmuştur. Bu tez çalışmasında, çamaşır makinalarında kullanılan fırçasız motorlar için bir sürücü tasarımı gerçekleştirilmiştir. Bu çalışmada, Alan Yönlendirmeli Kontrol (AYK) adı verilen bir algoritma kullanılarak yapılan sürücü tasarımı iki aşamadan oluşmaktadır. Birincisi, bahsedilen sürücünün modellenmesi ve simülasyonu, ikincisi ise deneysel çalışmadır.

Fırçasız motorlardan yüksek verim almanın en bilinen yolu Alan Yönlendirmeli Kontrol algoritması uygulamaktır. Alan Yönlendirmeli kontrolde gerilim kaynaklı çeviricinin ürettiği sinüsoidal sinyaller bazı karmaşık matematiksel dönüşümler kullanılarak doğru akıma çevrilmektedir. Çünkü referansı ve geribesleme girişi frekansa bağlı olmayan bir sisteme herhangi bir kontrolör uygulanması (PI vb...) daha kolay olmaktadır. Bu tez çalışmasında, hız ve tork kontrolü için sıkça kullanılan PI kontrolörün yanı sıra yeni bir kontrol tekniği olan Üssel Fonksiyon Kontrolü (ÜFK) de uygulanarak, PI kontrol sonuçlarıyla karşılaştırılmıştır.

Alan Yönlendirmeli Kontrol, karmaşık matematiksel dönüşümlerle çalışan bir algoritma olduğu için bu algoritmanın gerçek zamanlı olarak yürütülmesi ancak yüksek performansa sahip sayısal sinyal işlemci (DSP) tabanlı denetleyiciler ile mümkün olmaktadır. Tezin deneysel çalışma kısmında, böylesi güçlü bir DSP kabul edilen ve Texas Instrument firmasının C2000 tabanlı mikrodenetleyici ailesinin bir üyesi olan TMS320F28035 kullanılmıştır. Deney düzeneği, yine Texas Instrument firmasının HVDMC adlı kiti ile desteklenmiştir.

Modelleme ve simülasyon çalışmaları ise MATLAB/Simulink ortamında gerçekleştirilmiştir.

SYMBOLS

L_d	: d-axis Inductance
L_q	: q-axis Inductance
θ_r	: rotor electrical angle
ω_r	: rotor speed
λ_d	: d-axis magnetic flux
λ_q	: q-axis magnetic flux
Λ_m	: rotor magnetization constant
θ_r	: rotor electrical angle
ω_r	: rotor speed

ABBREVIATIONS

BEMF	: Back Electromotive Force
BLDC	: Brushless Direct Current Motor
BLM	: Brushless Motor
CT	: Clarke Transformation
FOC	: Field Oriented Control
ICT	: Inverse Clarke Transformation
IPT	: Inverse Park Transformation
PBC	: Power Function Based Controller
PMSM	: Permanent Magnet Synchronous Motor
PI	: Proportional Integral
PT	: Park Transformation
RPM	: Rotate Per Minute
SMO	: Sliding Mode Observer
SMCO	: Sliding Mode Current Observer
SVPWM	: Space Vector Pulse Width Modulation
VSI	: Voltage Source Inverter
VC	: Vector Control
WM	: Washing Machine

LIST OF FIGURES

Figure 2.1 Basic Flowchart of a WM Operation.....	3
Figure 2.2 Speed and torque characteristics of WM in wash and rinsing cycles [8].	4
Figure 2.3 Speed and Torque characteristic at distributing cycle and spinning- drying cycle [8]	5
Figure 3.1 A classification of AC Motor Types	6
Figure 3.2 Cross-sectional image of a PMSM/BLDC motor	7
Figure 3.3 Distributed Winding and Concentrated Winding	8
Figure 4.1 Schematic Diagram of Permanent Magnet Synchronous Motor [14] .	10
Figure 4.2 Electrical Equivalent of a 3-phase PMSM	11
Figure 4.3 Phasor Diagram of Clarke Transformation.....	13
Figure 4.4 PMSM equivalent circuit in d-q axis	16
Figure 4.5 Park transformation phasor diagram.....	17
Figure 5.1 Inverter Operating Principle [17]	21
Figure 5.2 Three phase VSI with a Y-type Connected Load	22
Figure 5.3 Signal forms of bipolar SPWM	24
Figure 5.4 Simplified 3-phase VSI.....	25
Figure 5.5 Space Vectors with their direction and magnitude	26
Figure 5.6 A sample reference vector to be emulated.....	27
Figure 5.7 Reference Voltage and its component in dq axis	29
Figure 5.8 Two adjacent vectors composing the reference vector.....	30
Figure 5.9 Switching patterns and corresponding switching time durations [25]	32
Figure 6.1 Block Diagram of FOC.....	35
Figure 6.2 Sensor Outputs of the Position Sensor Types	37
Figure 6.3 Classification of sensorless position detection methods for PMSM drive [32].....	38
Figure 6.4 Rotor flux position estimator based on SMO [34]	39
Figure 6.5 Control Loops in FOC.....	42
Figure 6.6 PI controller block diagram.....	43
Figure 6.7 Variation in exponent for different error values at a constant gain	44

Figure 6.8 Variation in the error with different gain values at constant λ	45
Figure 7.1 Simulink Schematic of modeled PMSM	47
Figure 7.2 Comparative Simulation Study Overview.....	48
Figure 7.3 Constant Torque applied to the PMSM	49
Figure 7.4 Variable Torque Load applied to the system.....	49
Figure 7.5 The Reference Speed	50
Figure 7.6 Comparative simulation results for the speed control for case 1	51
Figure 7.7 Comparative simulation results of the torque control for the case 1...52	
Figure 7.8 Controller outputs for case 1	53
Figure 7.9 Comparative simulation results of the speed control for case 2.....	54
Figure 7.10 Comparative simulation results of the torque control for case 2	54
Figure 7.11 Controller outputs for case 2	55
Figure 8.1 Main Stages of the Kit	56
Figure 8.2 The Driver Circuit	58
Figure 8.3 Experimental Setup	60
Figure 8.4 Flowchart of the proposed FOC algorithm	61
Figure 8.5 T_a , T_b and T_c and T_b - T_c signals of SVPWM Generator.....	62
Figure 8.6 Reference Speed Graphic of PMSM motor.....	62
Figure 8.7 Open Loop I_a and I_b currents in unloaded drum	63
Figure 8.8 Open Loop I_a and I_b currents in 8kg loaded drum	63
Figure 8.9 The estimated rotor angle	64
Figure 8.10 I_a , I_b currents and rotor angle at closed loop control for unloaded drum	64
Figure 8.11 I_a , I_b currents and rotor angle at closed loop control for 8kg loaded drum	65
Figure 8.12 I_a , I_b currents and rotor angle at closed loop control for unbalanced drum	65
Figure A..1 PBC controller, IPT and SVPWM blocks	71
Figure A..2 abc to dq-model block in PMSM model	71
Figure A..3 Mechanical modeling block of PMSM.....	71
Figure B..1 Block diagram of DSP TMS320F28035	72

LIST OF TABLES

Table 5.1. Switching States of Three Phase VSI.....	23
Table 5.2. Vectors and Corresponding Phases.....	26
Table 5.3. Voltage Vectors and corresponding voltage.....	28
Table 5.4. Switching calculations of transistors for all sectors.....	33
Table 7.1. PMSM Parameters.....	46
Table 7.2 Simulation Cases.....	49

1. INTRODUCTION

Brushless electric motor technology has been developed rapidly during the past few decades. Because of their various advantages over other types, brushless motors (BLDC and PMSM) have become one of the most preferred electric motors which are widely used in many applications. In addition to their use in the industrial field, they are also used in household appliances. Reduced size, high performance, very good controllability in full speed operating range and high efficiency [1] are some of the reasons to prefer brushless motors. For all these reasonable properties, brushless motors are started to dominate in some household appliances such as washing machines (WM), refrigerators and dishwashers. Therefore, this thesis deals with a proper driver design for a brushless motor that is used in Washing Machines. Besides their advantages, one problem arises in the usage of brushless motors. They need to be commutated electronically and it requires a suitable driver design to obtain maximum efficiency. Some driving techniques have been developed in years. Studies shows that Field Oriented Control (FOC), an algorithm to drive brushless motors, achieves one of the best performances in compared to some others in terms of speed and torque responses [2-4].

Permanent Magnet Synchronous Motors (PMSM) and Brushless Direct Current Motors (BLDC) are the main types of Brushless DC Electric Motors. They have many similarities. A BLDC and a PMSM motor both consists of a rotating permanent magnet which is called the rotor and surrounded by three equally spaced fixed windings which is called the stator. The main difference in these two motors is that the PMSM and the BLDC have sinusoidal and trapezoidal back EMFs, respectively. This is due to their stator winding arrangement type [5]. Since both are used in washing machines by manufacturers alternatively, PMSM motor is studied in this thesis.

Besides all the benefits mentioned above, one of the main reasons using BLMs in WMs is the noise level of operation. Since brushless motors have a very low noise level while operating, manufacturers are started to prefer these kinds of motors in WMs, in order to present more life quality to the customer.

The FOC algorithm, also called Vector Control, is applied to a three-phase

inverter such as Voltage Source Inverter (VSI) in order to control the stator current quantities (e.g. magnitude, phase, and frequency) of brushless motors. Furthermore, the FOC's theory is generally based on modeling brushless motors in the rotating reference frame, also known as the d-q reference frame [6]. By applying Clarke and Park transformations, the model can be easily converted to a d-q model. Once a d-q model is obtained one of the conventional control schemes (generally PI) is chosen to control the d and q DC input quantities. Clarke and Park transformations have heavy computations to execute in real time. Thus, powerful microcontrollers is needed to be chosen for the operation. In this thesis, Texas Instruments C2000 microcontrollers based motor kit is used for a digital implementation of the FOC algorithm.

The main objective of this thesis is to design a suitable driver based on FOC, to control the speed and torque of a PMSM for a washing machine. This driver design consists of two main parts: Modeling/simulation and digital implementation. Modeling and driver control simulations are implemented in Matlab/Simulink environment. The digital implementation is conducted in Texas Instrument Kit. In order to control the quantities of speed, torque, and flux, PI control is frequently used in the FOC algorithm. Now, in this study, a new control method named Power Function Based Control (PBC) is used to control those quantities and compared the results to each other.

The structure of the thesis study is given below. The study addresses modeling, simulation and digital implementation of a PMSM used in a WM. Chapter 2 gives a brief explanation regarding working cycles of an automatic WM. In chapter 3, brushless motors are discussed in details. Chapter 4 includes the PMSM modeling study with different coordinate frames and Clarke-Park transformations. Inverter topologies and modulation types are summarized in Chapter 5. Chapter 6 introduces PMSM Drive with the sensorless control scheme. Chapter 7 and 8 present simulation study and digital implementation, respectively. Chapter 9 summarizes the results obtained from the experimental setup. Finally, chapter 10 comments the results and evaluates the whole thesis study.

2. WASHING MACHINE

Operation of an automated Washing Machine are generally divided into four main cycles, as shown in Fig. 2.1. Washing cycle is the first step of operation which the laundry is cleaned by using tumbling force, water and detergent. The second one is called rinsing cycle in which the laundry is rinsed by water to remove detergent and other kind of cleaning agents. The third cycle is the distribution cycle in where the laundry is tumbled at low-range speed without using water. This cycle is relatively shorter than all others and it is a preparation of the fourth one. It is aimed to reduce unbalanced load that could occur in the spinning-drying cycle. Spinning-drying cycle is the last cycle where usually lasts around 10 to 20 mins. By using centrifugal force, the water absorbed by the laundry in previous cycles, is extracted in this cycle. [7]

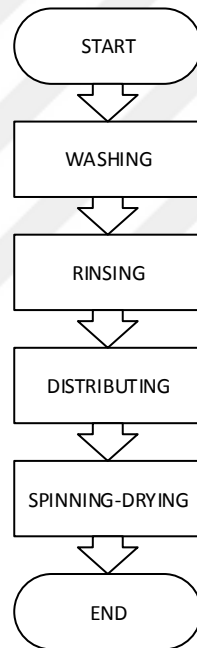


Figure 2.1 Basic Flowchart of a WM Operation

2.1. Operation Cycles in a Washing Machine

As this thesis deals with the PMSM driver design for a washing machine, the control of the machine is addressed in terms of speed and torque. The PMSM provides different rotational speeds and torques to the drum in each cycle.

2.1.1. Washing cycle

A washing machine's primary cycle is the washing cycle. It also has the longest working duration. This is the cycle where clothes are tumbled at motor's low speed-range with water and detergent. Depending on the program chosen by the end user, it usually takes 30 to 60 minutes to complete. During washing cycle, drum is rotated in a constant speed of 40 to 80 RPM. Since the laundry placed at the bottom of drum, pumped water and added cleaning agents are all together in the beginning of this cycle, it causes relatively big load at start-up of the motor. As the drum rotates, this big load is started to falls down [7]. Torque and speed characteristic at washing and rinsing cycles is shown Fig. 2.2 Note that there are fluctuations at both speed and torque graphics due to tumbling operation.

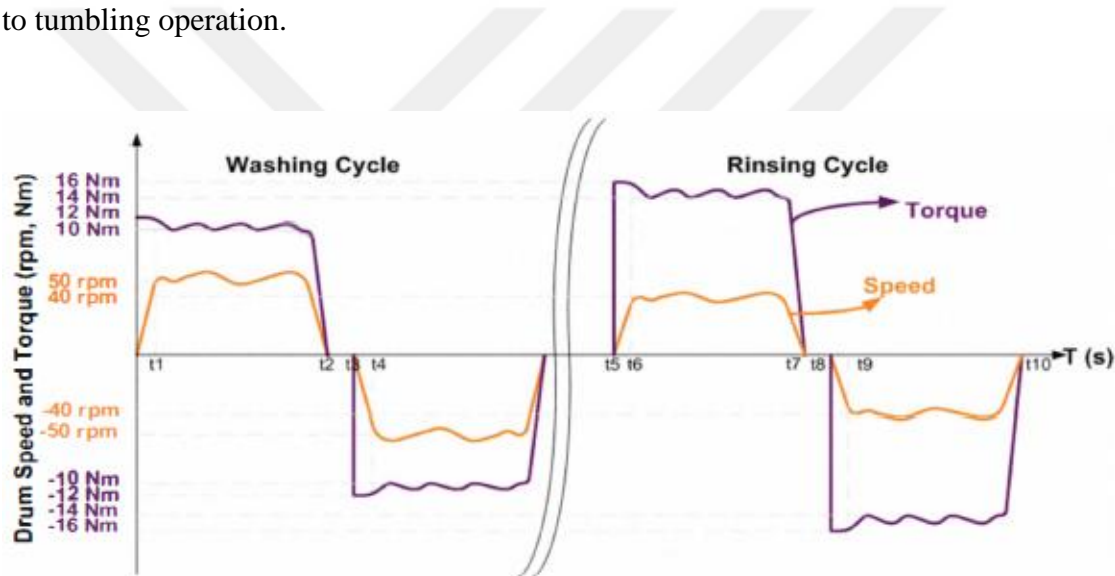


Figure 2.2 Speed and torque characteristics of WM in wash and rinsing cycles [8].

2.1.2. Rinsing cycle

In the rinsing cycle, more water is pumped to the drum in order to extract detergent from the laundry. This operation is conducted multiple times to ensure lack of detergent at the laundry. As water is more than the previous cycle, the load will be bigger so the laundry will try to act like a more linearly load and it causes slightly fewer fluctuations at torque graphic in compared to washing cycle does. The speed characteristic also does not change much than in the washing cycle. Maybe one difference is worth to state that rinsing speed is slightly slower than washing speed. This

causes more difficulties in terms of low-speed operation region of PMSM particularly when high loads occur [7]. The speed and torque characteristics at the rinsing cycle are shown in Fig. 2.2

2.1.3. Distributing cycle

After washing and rinsing cycles, laundry congregates at the inner surface of the drum with the help of water and tumbling operation. This big mass of clothes causes unbalanced load at higher drum speed where occurs in a spinning-drying cycle. Thus, distributing laundry is a must just before the spinning-drying cycle. Drum speed at this cycle is around 100rpm. This cycle is also the shortest one among all, ending up to 3 minutes. Since water in the drum is drained out in the distribution cycle, the load is less small than previous cycles. The torque characteristics of the distribution cycle and the spinning-drying cycle are shown in Fig. 2.3. As can be seen, as the load is smaller now, torque is considerably decreased.

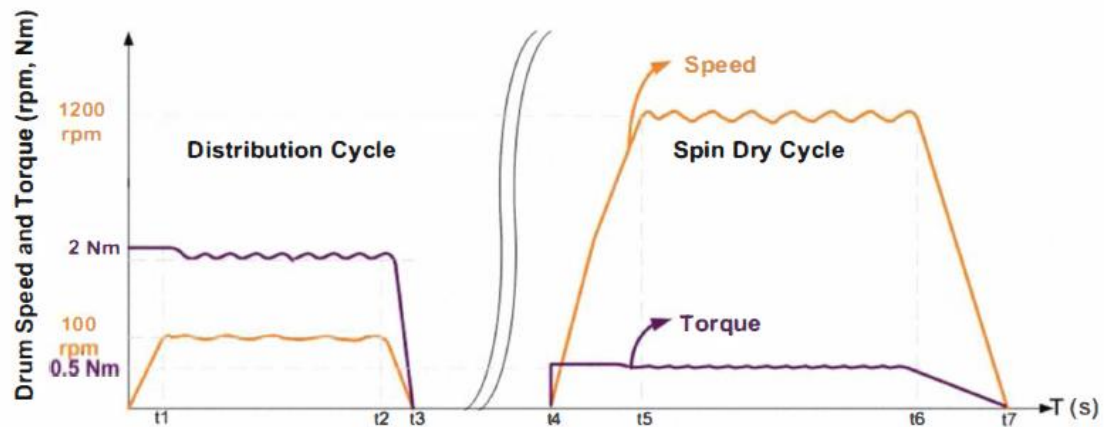


Figure 2.3 Speed and Torque characteristic at distributing cycle and spinning-drying cycle [8]

2.1.4. Spinning-drying cycle

The last cycle of a washing machine operation is a spinning-drying cycle. Distribution cycle could reduce the unbalanced load, yet it is not able to remove it completely. Thus, fluctuations at torque will be larger than ever due to unbalance the load and very high drum speed. The load and speed characteristics are shown in Fig. 2.3. Note that spinning-drying cycle has the highest drum speed which could reach up to 1600 rpm.

3. PERMANENT MAGNET MOTORS

There are plenty of methods regarding the classification of electric motors in terms of various specifications and some of them are really sophisticated. Nevertheless, electric motors can be divided into two main categories according to their voltage source: DC motors and AC motors. Since DC motors are out of the scope of this study, it will not be discussed here. A simplified classification of AC electric motors [9, 11] can be seen in Fig. 3.1.

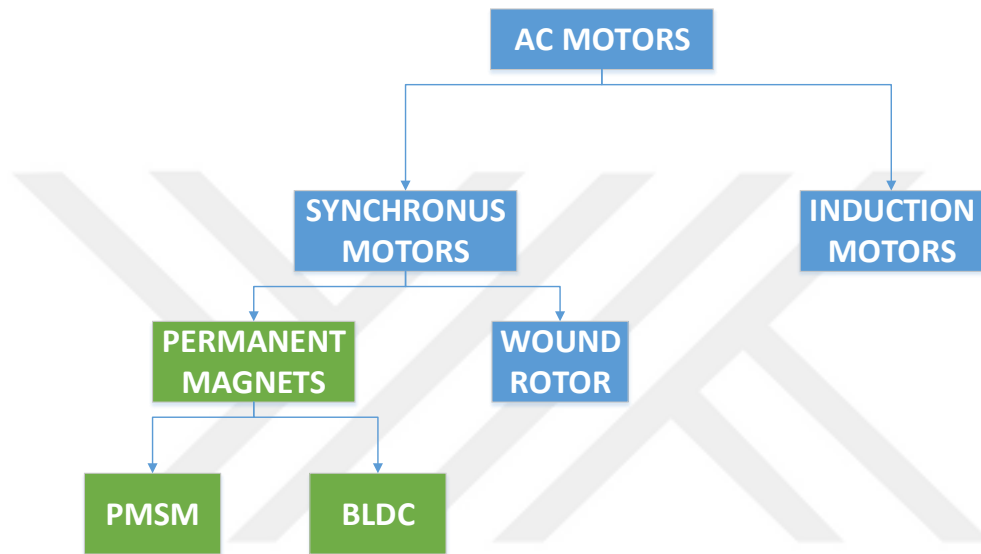


Figure 3.1 A classification of AC Motor Types

As can be seen in Figure 3.1, Permanent Magnet Synchronous Motors (PMSM) and Brushless DC motors (BLDC) are both permanent magnets and have windings of their stator.

3.1. Basic Structure

A cross-section of PMSM/BLDC motors is shown in Figure 3.2. It has a permanent magnet rotor and stator windings.

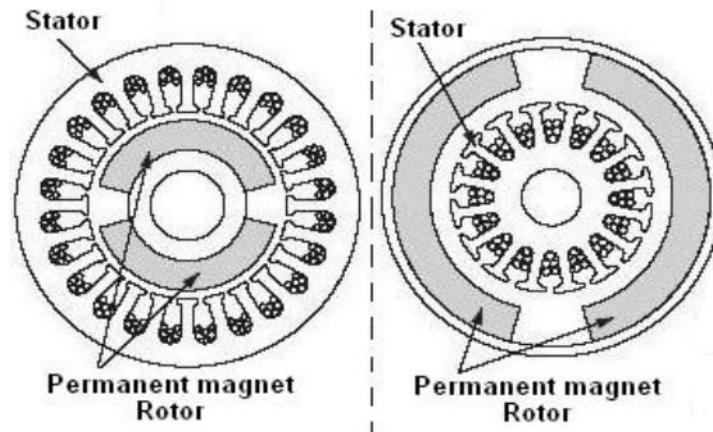


Figure 3.2 Cross-sectional image of a PMSM/BLDC motor

As indicated in Figure 3.2, PMSM/BLDC motors are manufactured in two different types according to how their permanent magnet rotors are mounted around the stator. If the rotor (magnet) is located inside the stator, it is called Interior Mounted Permanent Magnet (IPMSM), whereas if the rotor is placed outside the stator, it is called surface-mounted permanent magnet (SPMSM). Washing Machines generally use IPMSM [10].

A PMSM produces magnetic flux due to rotating permanent magnets in the rotor, which are motioned by the stators applying a synchronous rotational field. Moreover, the flux that is applied by the stators produces torque most effectively when it is orthogonal to flux generated by the rotors. The overall advantages of PMSM construction compared with conventional AC machine are [10]:

- Slip-rings free (no excitation winding)
- Losses due to copper is decreased (no excitation winding)
- Weight is lighter.
- Less heat and better heat dissipation
- Reduced size
- Lower torque ripple improves position control
- Better EMI
- Excellent torque at low speeds

Despite BLDC and PMSM motors have common similarities, there are still a few differences in respect to their structure and drive methods.

3.2. Differences Between BLDC and PMSM

BLDC and PMSM motors are both permanent magnet brushless motors. They both consist of a permanent magnet (the rotor) rotating about its axis and surrounded by three equally spaced fixed windings (the stator). Current flow in each winding produces a magnetic field vector, summing with the fields from the other windings.

The PMSM has a sinusoidal back EMF, whereas the BLDC has a trapezoidal back EMF as a result of their winding arrangement. Despite both of them have a permanent magnet rotor, the difference is in the winding arrangement of the stator and shaping of the magnets. PMSM has distributed stator winding whereas BLDC has concentrated stator winding which is shown in Figure 3.3 [12].

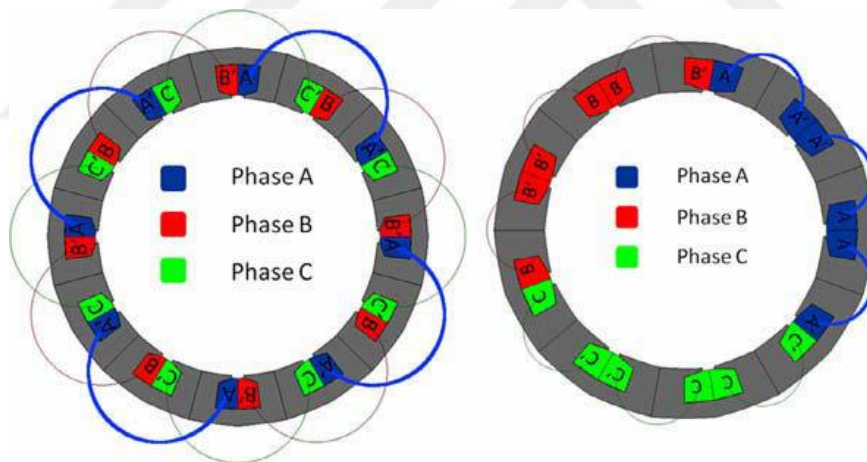


Figure 3.3 Distributed Winding and Concentrated Winding

In order to obtain smooth sinusoidal BEMF waveform, conductors are placed in several slots under single pole. This armature winding is known as distribute winding which is shown the left side of Figure 3.3. Concentrated winding is used where number of slots on the armature is equal to number of poles in the machine. This armature winding of alternator gives non-sinusoidal BEMF.

One of the important difference is that sinusoidal stator currents are needed to produce a steady state torque in the PMSM, whereas rectangular-shaped currents are needed to produce a steady state torque in the BLDC [11].

There are also important differences in their driving methods. BLDC motors are generally driven by a trapezoidal (also called six-step switching) control which is relatively simple. However, trapezoidal control contains harmonics and these harmonics cause electrical and audible noise. Although electrical noise is easy to eliminate using low pass filters, this not the case for the audible noise, which is not desired for the end user's comfort [7]. Another weakness of trapezoidal control is having high torque ripples, especially at low speeds.

Furthermore, the trapezoidal control is not an efficient method to control a washing machine's motor in terms of the dynamic response. Because the torque load in the drum changes dynamically during the operation of WM. It can also vary with different types of loads and by selected washing program. Also, the gravitational force resists the motor, while the laundry is on the top side of the drum. Instead of trapezoidal control, more complex algorithms such as Field Oriented Control (FOC) can overcome this dynamical changes at the load [13].

4. PMSM MODELING

To realize the FOC algorithm for a PMSM, the motor must be modeled first and the first step in modeling is to know the electrical and mechanical structure.

As mentioned in the previous chapter, the PMSM has a permanent magnet as the rotor which creates a magnetic field and the stator has three-phase windings which are assembled on it such a way that the corresponding currents flow by 120° phase difference between each other. The structure of PMSM and current axis are shown in Figure 4.1 [14].

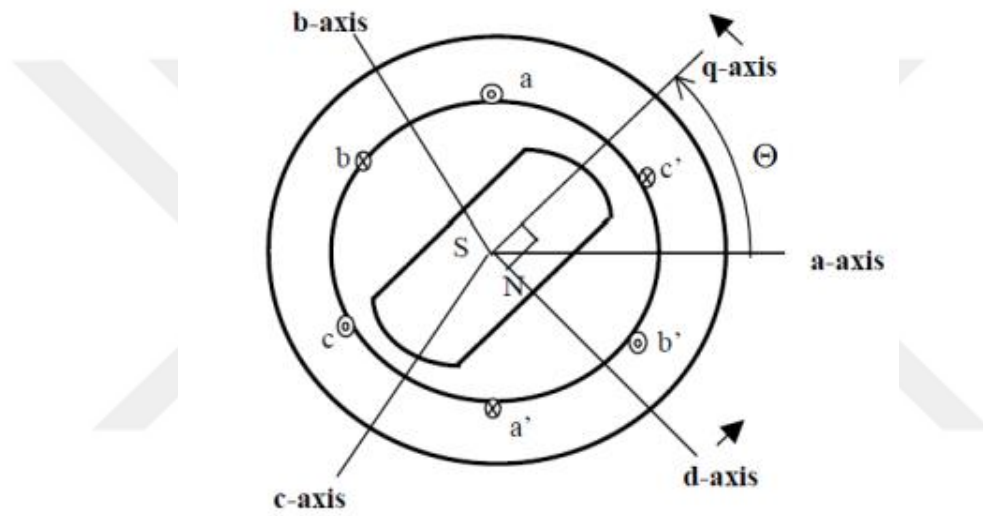


Figure 4.1 Schematic Diagram of Permanent Magnet Synchronous Motor [14]

In Figure 4.1, a , b , c axes are the axes of the three-phase stator windings. The d -axis is chosen in the flux direction of the permanent magnet, whereas the q -axis is perpendicular to the d -axis, keeping 90° ahead of it [14].

Faraday's Law states that changing the magnetic field induces a voltage across a wire. Correspondingly, the permanent magnet in the rotor induces voltage in the stator windings, as the rotor keeps rotating. This is called the back electromotive force (BEMF). The stator windings have also their own resistances and inductances, due to the coils made up of the windings. Using this knowledge, the PMSM could be modeled. In this thesis, following assumptions and limitations are considered while modeling [15]:

- Stator windings produce sinusoidal MMF distribution. Space harmonics in the air-gap are neglected.
- Air-gap reluctance has a constant component
- Three-phase sinusoidal voltages and corresponding windings are balanced
- Hysteresis and eddy currents are neglected.

It should note that, since washing machines which have brushless motor are generally manufactured by using Interior Permanent Magnet Synchronous Motor (IPMSM) due to its robustness in high speeds, IPMSM modeling will be realized in the next sections. In surface-mounted PMSM (SPMSM), magnets are generally fixed on the rotor surface by using an epoxy glue. Therefore, the mechanical strength of the SPMSM depends on the chemical performance of epoxy glue, in circumstances where any retaining sleeve is not used. Hence, IPMSM machines have a more robust structure and preferred to be used in high-speed applications [11].

4.1. Electrical Equivalent of PMSM

The electrical equivalent of a three phase PMSM can be represented in Figure 4.2.

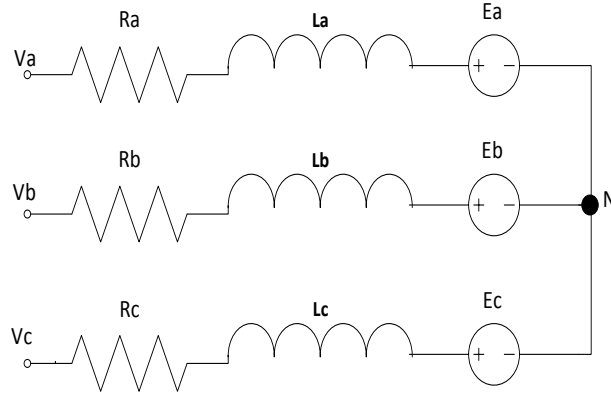


Figure 4.2 Electrical Equivalent of a 3-phase PMSM

The electrical circuit part of PMSM model can be stated as

$$\begin{bmatrix} V_a \\ V_b \\ V_c \end{bmatrix} = \begin{bmatrix} R_a & 0 & 0 \\ 0 & R_b & 0 \\ 0 & 0 & R_c \end{bmatrix} \begin{bmatrix} i_a \\ i_b \\ i_c \end{bmatrix} + p \begin{bmatrix} \lambda_a \\ \lambda_b \\ \lambda_c \end{bmatrix} \quad (4.1)$$

where V_a, V_b, V_c , are the per phase stator voltages, $R_a = R_b = R_c = R$ are the per phase stator resistances, i_a, i_b, i_c are the per phase stator currents and λ_a, λ_b , and λ_c are the stator flux linkages and p stands for $\frac{d}{dt}$.

The stator currents i_a, i_b and i_c can be defined in matrix form as

$$\begin{bmatrix} i_a \\ i_b \\ i_c \end{bmatrix} = |\vec{I}_s| \cdot \begin{bmatrix} \sin wt \\ \sin(wt - \frac{2\pi}{3}) \\ \sin(wt + \frac{2\pi}{3}) \end{bmatrix} \quad (4.2)$$

Where $|\vec{I}_s|$ is the magnitude of stator current, w is the stator field's frequency. The flux linkages λ_a, λ_b and λ_c can be expressed as

$$\begin{bmatrix} \lambda_a \\ \lambda_b \\ \lambda_c \end{bmatrix} = L \cdot \begin{bmatrix} i_a \\ i_b \\ i_c \end{bmatrix} + \begin{bmatrix} \Lambda_m \sin wt \\ \Lambda_m \sin(wt - \frac{2\pi}{3}) \\ \Lambda_m \sin(wt + \frac{2\pi}{3}) \end{bmatrix} \quad (4.3)$$

Where Λ_m is the constant flux vector and L is the self-inductance of each stator winding ($L_a = L_b = L_c = L$). From Eq (4.1) it is clear that derivative of λ_{abc} must be defined to model the PMSM. Taking the derivative of Eq.(4.3)

$$p \begin{bmatrix} \lambda_a \\ \lambda_b \\ \lambda_c \end{bmatrix} = L \cdot p \begin{bmatrix} i_a \\ i_b \\ i_c \end{bmatrix} + \begin{bmatrix} \Lambda_m \cdot w \cdot \cos \Theta \\ \Lambda_m \cdot w \cdot \cos(\Theta - \frac{2\pi}{3}) \\ \Lambda_m \cdot w \cdot \cos(\Theta + \frac{2\pi}{3}) \end{bmatrix} \quad (4.4)$$

Finally, substituting Eq. (4.4) into Eq. (4.1) and rearranging the matrix, the model equation can be expressed as

$$\begin{bmatrix} V_a \\ V_b \\ V_c \end{bmatrix} = \begin{bmatrix} R \cdot i_a + L \cdot p \cdot i_a + \Lambda_m \cdot w \cdot \cos \Theta \\ R \cdot i_b + L \cdot p \cdot i_b + \Lambda_m \cdot w \cdot \cos(\Theta - \frac{2\pi}{3}) \\ R \cdot i_c + L \cdot p \cdot i_c + \Lambda_m \cdot w \cdot \cos(\Theta + \frac{2\pi}{3}) \end{bmatrix} \quad (4.5)$$

It can be stated from Eq. (4.5) that voltage and current of each phase have differential equations. It means there is non-linearity. In order to use linear control structures efficiently, non-linearity must be eliminated. This could occur by making the equations linear. This linearity process could be realized by applying some transformations which will be defined in the next sections.

4.2. Stationary ($\alpha\beta$) Reference Frame

In the previous section, the dynamic model of the PMSM is obtained in terms of the voltage equations and flux linkage equations. The inductance is time-dependent. Furthermore, as the rotor keeps rotating, the variables of the model are also time-varying. Hence, for reducing the complexity of the dynamic model, Clarke and Park's transformations are needed to be applied to converting the abc reference frame of PMSM model into the $\alpha\beta$ -reference frame is realized by the Clarke transformation (CT), which is illustrated in the diagram of Figure 4.3.

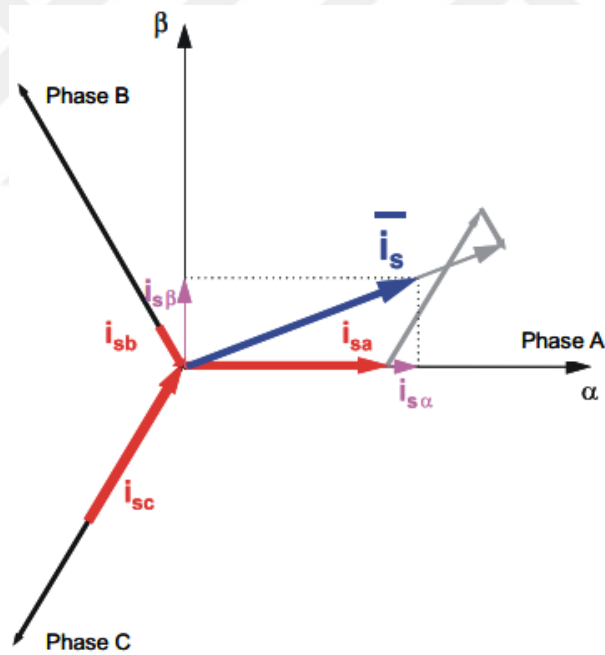


Figure 4.3 Phasor Diagram of Clarke Transformation

The vector diagram in Figure 4.3 indicates that the resultant (reference) vector \bar{i} is the vectorial summation of three phase currents i_a , i_b , i_c . By applying Clarke Transformation to the phase currents, the resultant vector \bar{i} could be represented by two orthogonal vectors i_α and i_β . Note that the CT converts a three-axis system into a two-axis

system without any change in the stator reference vector. The CT matrix is described as

$$T_{\alpha\beta\gamma} = \frac{2}{3} \begin{bmatrix} 1 & -\frac{1}{2} & -\frac{1}{2} \\ 0 & \frac{\sqrt{3}}{2} & -\frac{\sqrt{3}}{2} \\ \frac{\sqrt{2}}{2} & \frac{\sqrt{2}}{2} & \frac{\sqrt{2}}{2} \end{bmatrix} \quad (4.6)$$

Note that γ is not included to the transformation. It is just added to make transformation matrix reversible. The Inverse Clarke transformation (ICT) matrix, $T_{\alpha\beta\gamma}^{-1} = T_{abc}$, is stated as

$$T_{abc} = \begin{bmatrix} 1 & 0 & 1 \\ -\frac{1}{2} & \frac{\sqrt{3}}{2} & 1 \\ -\frac{1}{2} & -\frac{\sqrt{3}}{2} & 1 \end{bmatrix} \quad (4.7)$$

ICT matrix is used when it is desired to convert two-phase reference system back into three-phase reference system because calculating PWM durations for switching VSI requires three phase currents as explained in chapter 5 of this thesis.

Applying CT to the phase voltages in Eq. (4.1), the phase-voltage matrix in $\alpha\beta$ -reference frame is obtained as

$$\begin{bmatrix} V_\alpha \\ V_\beta \\ V_0 \end{bmatrix} = \frac{2}{3} \begin{bmatrix} 1 & -\frac{1}{2} & -\frac{1}{2} \\ 0 & \frac{\sqrt{3}}{2} & -\frac{\sqrt{3}}{2} \\ \frac{\sqrt{2}}{2} & \frac{\sqrt{2}}{2} & \frac{\sqrt{2}}{2} \end{bmatrix} \begin{bmatrix} R & 0 & 0 \\ 0 & R & 0 \\ 0 & 0 & R \end{bmatrix} \begin{bmatrix} i_a \\ i_b \\ i_c \end{bmatrix} + p \begin{bmatrix} \lambda_a \\ \lambda_b \\ \lambda_c \end{bmatrix} \quad (4.8)$$

After multiplication of matrices and cancelling zero element, the equation can be finally simplified as

$$\begin{bmatrix} V_\alpha \\ V_\beta \end{bmatrix} = \begin{bmatrix} R \cdot i_a + p \cdot \lambda_a \\ \frac{1}{\sqrt{3}} \{ R \cdot (i_b - i_c) + p \cdot \lambda_b - p \lambda_c \} \end{bmatrix} \quad (4.9)$$

If CT is applied to the phase currents equation is given by

$$\begin{bmatrix} i_\alpha \\ i_\beta \end{bmatrix} = \begin{bmatrix} i_a \\ \frac{1}{\sqrt{3}} (i_b - i_c) \end{bmatrix} \quad (4.10)$$

If CT is applied to the stator flux linkages, then equation is given by

$$\begin{bmatrix} \lambda_\alpha \\ \lambda_\beta \end{bmatrix} = \begin{bmatrix} \lambda_a \\ \frac{1}{\sqrt{3}} (\lambda_b - \lambda_c) \end{bmatrix} \quad (4.11)$$

By substituting the converted currents in Eq (4.10) and the converted flux linkages in Eq. (4.11) into Eq. (4.9), $\alpha\beta$ reference frame model can be expressed as

$$\begin{bmatrix} V_\alpha \\ V_\beta \end{bmatrix} = \begin{bmatrix} R \cdot i_a + p \cdot \lambda_a \\ \frac{1}{\sqrt{3}} \{ R \cdot \sqrt{3} i_\beta + p \cdot \sqrt{3} \lambda_b \} \end{bmatrix} \quad (4.12)$$

After simplification, transformation eventually will be

$$\begin{bmatrix} V_\alpha \\ V_\beta \end{bmatrix} = \begin{bmatrix} R & 0 \\ 0 & R \end{bmatrix} \begin{bmatrix} i_\alpha \\ i_\beta \end{bmatrix} + p \begin{bmatrix} \lambda_\alpha \\ \lambda_\beta \end{bmatrix} \quad (4.13)$$

As clearly seen from Eq. (4.13) and Eq. (4.1), they are very similar to each other even though they are in different reference frames: abc and $\alpha\beta$, respectively. Using this similarity, the flux linkage equation in $\alpha\beta$ frame can be written as

$$\begin{bmatrix} \lambda_\alpha \\ \lambda_\beta \end{bmatrix} = L \cdot \begin{bmatrix} i_\alpha \\ i_\beta \end{bmatrix} + \begin{bmatrix} \Lambda_m \cos \Theta \\ \Lambda_m \sin \Theta \end{bmatrix} \quad (4.14)$$

Similarly, the derivative of the flux linkage equation in $\alpha\beta$ frame can be written

as

$$p \begin{bmatrix} \lambda_\alpha \\ \lambda_\beta \end{bmatrix} = L \cdot p \begin{bmatrix} i_\alpha \\ i_\beta \end{bmatrix} + \begin{bmatrix} -w \cdot \Lambda_m \sin \Theta \\ w \Lambda_m \cos(\Theta) \end{bmatrix} \quad (4.15)$$

Finally, inserting Eq. (4.15) into Eq. (4.13), the mathematical model of the PMSM in the $\alpha\beta$ -frame can be stated as

$$\begin{bmatrix} V_\alpha \\ V_\beta \end{bmatrix} = \begin{bmatrix} R & 0 \\ 0 & R \end{bmatrix} \begin{bmatrix} i_\alpha \\ i_\beta \end{bmatrix} + L \cdot p \begin{bmatrix} i_\alpha \\ i_\beta \end{bmatrix} + \begin{bmatrix} -w \cdot \Lambda_m \sin \Theta \\ w \Lambda_m \cos(\Theta) \end{bmatrix} \quad (4.16)$$

4.3. dq Rotating Reference Frame

To model the motor on d-q axis (*dq* reference frame), it needs two sets of equivalent circuits which represent the parameters in two axes: one along the d axis and the other along the q axis [16] as shown in Figure 4.4. The dynamic model of a PMSM can be obtained in the dq reference frame by applying Park Transformation.

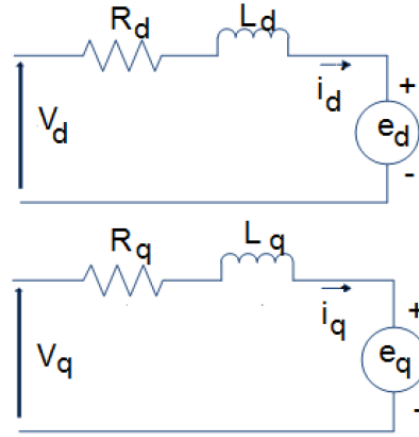


Figure 4.4 PMSM equivalent circuit in d-q axis

The PT (the dq0 transform), can be assumed as an extension of the CT, introduced in the previous section. In PT, an angle transformation is realized to transform voltage or current variables in the stationary reference frame to the rotating reference frame. The synchronous or rotating reference frame can be aligned to rotate with the voltage (VSI) or with the current (CSI). The phasor diagram of PT can be seen in Figure 4.5.

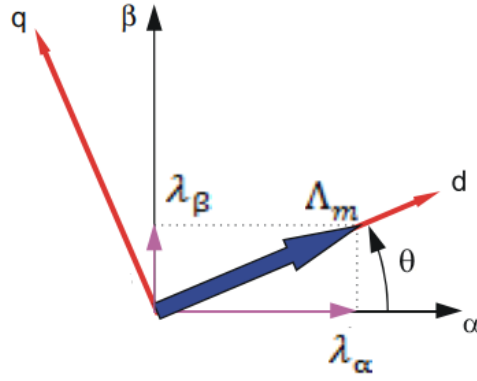


Figure 4.5 Park transformation phasor diagram

The PT provides a rotating coordinate system (the dq-reference frame). If this frame rotates by the same frequency with the synchronous frequency, as the current itself, the AC current in the $\alpha\beta$ -axis behaves like DC current in the dq -axis [7]. The PT matrix is given by

$$T_{dq0} = \begin{bmatrix} \cos \theta & \sin \theta \\ -\sin \theta & \cos \theta \end{bmatrix} \quad (4.17)$$

The voltage equations for V_d and V_q can be defined as

$$\begin{bmatrix} V_d \\ V_q \end{bmatrix} = T_{dq0} \cdot \begin{bmatrix} V_\alpha \\ V_\beta \end{bmatrix} \quad (4.18)$$

Similarly, the current equations can be written as

$$\begin{bmatrix} I_d \\ I_q \end{bmatrix} = \begin{bmatrix} \cos \theta & \sin \theta \\ -\sin \theta & \cos \theta \end{bmatrix} \cdot \begin{bmatrix} I_\alpha \\ I_\beta \end{bmatrix} \quad (4.19)$$

Once the multiplication is done, the conversion will be

$$\begin{bmatrix} I_d \\ I_q \end{bmatrix} = \begin{bmatrix} I_\alpha \cos \theta & + & I_\beta \sin \theta \\ -I_\alpha \sin \theta & + & I_\beta \cos \theta \end{bmatrix} \quad (4.20)$$

For the PMSM model, remind that the derivatives of currents were introduced in the previous chapter. Taking the derivative of each side in Eq. (4.20), following result will occur as

$$p \begin{bmatrix} I_d \\ I_q \end{bmatrix} = \begin{bmatrix} p I_\alpha (\cos \Theta) & + p I_\beta (\sin \Theta) & + & \omega (I_\alpha \cos \Theta + I_\beta \sin \Theta) \\ -p I_\alpha (\sin \Theta) & + p I_\beta (\cos \Theta) & - & \omega (-I_\alpha \sin \Theta + I_\beta \cos \Theta) \end{bmatrix} \quad (4.21)$$

Finally, inserting the identifiers I_d and I_q of Eq (4.20) is into Eq (4.21) the equations can be expressed as

$$p \begin{bmatrix} I_d \\ I_q \end{bmatrix} = \begin{bmatrix} p I_\alpha (\cos \Theta) & + p I_\beta (\sin \Theta) & + & \omega I_d \\ -p I_\alpha (\sin \Theta) & + p I_\beta (\cos \Theta) & - & \omega I_q \end{bmatrix} \quad (4.22)$$

Similarly, the voltage equations can be written as

$$\begin{bmatrix} V_d \\ V_q \end{bmatrix} = \begin{bmatrix} \cos \Theta & \sin \Theta \\ -\sin \Theta & \cos \Theta \end{bmatrix} \cdot \begin{bmatrix} V_\alpha \\ V_\beta \end{bmatrix} \quad (4.23)$$

Substituting Eq. (4.16) into Eq. (4.23), the resultant equations will become

$$\begin{bmatrix} V_d \\ V_q \end{bmatrix} = \begin{bmatrix} \cos \Theta & \sin \Theta \\ -\sin \Theta & \cos \Theta \end{bmatrix} \cdot \left\{ \begin{bmatrix} R & 0 \\ 0 & R \end{bmatrix} \begin{bmatrix} i_\alpha \\ i_\beta \end{bmatrix} + L \cdot p \begin{bmatrix} i_\alpha \\ i_\beta \end{bmatrix} + \begin{bmatrix} -\omega_r \cdot \Lambda_m \sin \Theta \\ \omega_r \cdot \Lambda_m \cos \Theta \end{bmatrix} \right\} \quad (4.23)$$

Writing Eq. (4.23) explicitly and simplifying by using trigonometric identities, V_d and V_q can be rearranged, respectively as

$$V_d = R(i_\alpha \cos \Theta + i_\beta \sin \Theta) + L(p i_\alpha \cdot \cos \Theta + p i_\beta \cdot \sin \Theta) - \omega_r \cdot \Lambda_m \sin \Theta \cdot \cos \Theta + \omega_r \cdot \Lambda_m \cos \Theta \cdot \sin \Theta \quad (4.24)$$

$$V_d = R(i_\alpha \cos \Theta + i_\beta \sin \Theta) + L(p i_\alpha \cdot \cos \Theta + p i_\beta \cdot \sin \Theta) + \omega_r \cdot \Lambda_m (-\sin \Theta \cdot \cos \Theta + \cos \Theta \cdot \sin \Theta) \quad (4.25)$$

$$V_d = R(i_\alpha \cos \Theta + i_\beta \sin \Theta) + L \cdot p(p i_\alpha \cdot \cos \Theta + i_\beta \cdot \sin \Theta) \quad (4.26)$$

$$V_q = R(-i_\alpha \sin \Theta + i_\beta \cos \Theta) + L(-p i_\alpha \cdot \sin \Theta + p i_\beta \cdot \cos \Theta) + \omega_r \cdot \Lambda_m \sin^2 \Theta + \omega_r \cdot \Lambda_m \cos^2 \Theta \quad (4.27)$$

$$V_q = R(-i_\alpha \sin \Theta + i_\beta \cos \Theta) + L(-p i_\alpha \cdot \sin \Theta + p i_\beta \cdot \cos \Theta) + \omega_r \cdot \Lambda_m (\sin^2 \Theta + \cos^2 \Theta) \quad (4.28)$$

$$V_q = R(-i_\alpha \sin \theta + i_\beta \cos \theta) + L.p(-i_\alpha \sin \theta + i_\beta \cos \theta) + \omega_r \cdot \Lambda_m \quad (4.29)$$

Using Eq. (4.20) and Eq. (4.22) and placing the identifiers I_d and I_q into Eq. (4.26) and Eq. (4.29), the resultant model equations in the dq-frame can be simplified as

$$V_d = R.I_d + L.pI_d - \omega_r.L.I_q \quad (4.30)$$

$$V_q = R.I_q + L.pI_q - \omega_r.L.I_d + \omega_r \cdot \Lambda_m \quad (4.31)$$

Note that, once PT is applied, all current and voltage values are DC quantities now. Through this transformation, the non-linear mathematical expressions of a PMSM are transformed into a simple form which acting as a DC motor, thus effectively applying the linear control theory to the control of a PMSM [7].

4.4. Mechanical Dynamics of PMSM

A final step still remains to represent the complete dynamic model of a PMSM. The electromagnetic torque of a PMSM can be expressed as [24]

The developed torque is given by

$$T_e = \frac{3}{2}P(\lambda_f I_q + \lambda_d I_q - \lambda_q I_d) \quad (4.32)$$

The mechanical dynamics of the PMSM is usually expressed in the familiar form

$$J \frac{d\omega_r}{dt} = T_e - T_L - B\omega_r \quad (4.33)$$

Finally, rotor mechanical speed can be derived from Eq. (4.33)

$$\omega_r = \frac{1}{J} \int (T_e - T_L - B\omega_r) dt \quad (4.34)$$

And the rotor electrical speed is given by

$$\omega_e = \omega_r P \quad (4.35)$$

Where T_e - the electromechanical torque, P - the number of pole pairs, T_L - the load torque, B -viscous friction factor, and J -moment of inertia.



5. INVERTERS AND MODULATION TECHNIQUES

Except for the motor itself, the inverter circuit can be considered the only hardware part of the FOC. To control the switching durations of an inverter, modulation techniques must be used. In this chapter, after power inverters and modulation techniques have briefly introduced the study will focus on, in detail, one of the effective modulation techniques called Space Vector Pulse Width Modulation (SVPWM).

5.1. Inverters

An inverter is an electronic converter circuit consisting of active switching components such as IGBT and MOSFETS. Generally speaking, it is used to convert DC power to AC one. There are numerous purposes of using an inverter in applications. For instance, connecting DC power supplies of the solar, wind turbine, and fuel cell to the grid; transferring power to long-distance or controlling the frequency, the amplitude or the phase of the output waveform (current or voltage). Fig. 5.1 shows a basic block diagram of how to inverters work [17]. Since the DC sources are two types as the current and the voltage, the inverters are similarly classified by two types as Current Source Inverter (CSI) and Voltage Source Inverter (VSI) [6].

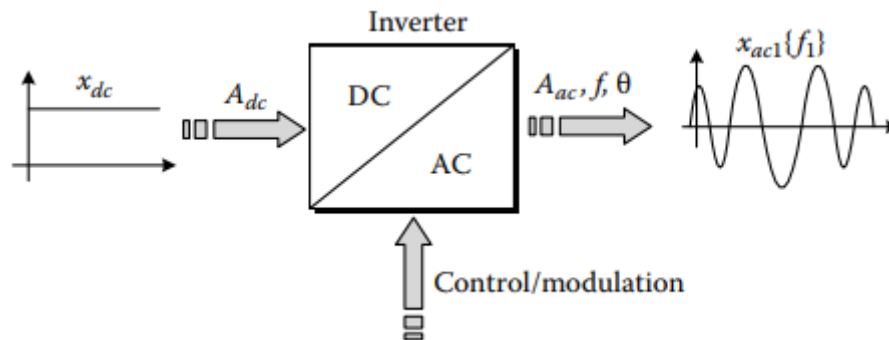


Figure 5.1 Inverter Operating Principle [17]

5.1.1. Current source inverters

Current source Inverters (CSI) generally has a constant current source and they consist an inductor in series with the DC bus for energy storage and ripple reduction of current signal. AC current quantities (e.g. magnitude, frequency and phase) can be

controlled by using a CSI. Current source inverters could be single or three phase. It is preferred in medium and high power applications.

5.1.2. Voltage source inverters

The voltage source inverters (VSI) may have constant or variable DC source. It is supplied by a DC Link consisting of a rectified voltage source and a capacitor. VSI is the most common power converter used in applications, requiring DC -AC power conversion. Especially in low and medium power, they may be used both in single and three-phase systems with the classic two-level topologies. Usage area of VSI varies widely. Some of them are uninterruptable power supplies (UPS), household appliances (washing machines, air conditioning, etc.), photovoltaic power conversion, adjustable speed drives, pumps, compressors, fans, and conveyors [17].

Common topologies of the VSI are half-bridge, H-bridge, and full-bridge (three-phase). Since the first two of them is out of scope, the operating principle of a three-phase inverter will be explained in detail. Figure 5.2 shows a three-phase VSI, using IGBTs as switching components.

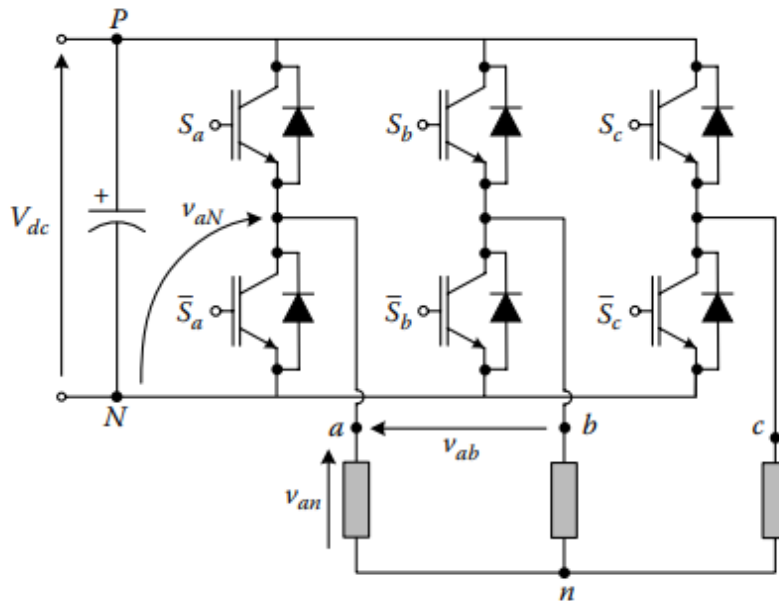


Figure 5.2 Three phase VSI with a Y-type Connected Load

Operating principle of a three-phase VSI is quite simple. Each three-leg has its own control signal being a binary value (0 or 1). S_a , S_b , and S_c are control signals of

upper switches and they could be only 1 or 0 where 1 represents the “ON state” of the related conducting switch and 0 the “OFF state” of (the switch is open). The lower switch of each leg is controlled with complementary signals of S_a , S_b , and S_c , respectively to prevent from short-circuiting the DC link due to conducting switches simultaneously, and to prevent from the undefined output voltages due to switches to be simultaneously open [17].

Since there are three legs and three control signals (S_a , S_b , S_c) for each of them, there will be $2^3 = 8$ different switching states and 8 phase voltages and space vectors which correspond to them, as listed in Table 5.1

Table 5.1. Switching States of Three Phase VSI

Switching State	Gating Signals			Output Voltage			Space Vector
	S_a	S_b	S_c	V_{an}	V_{bn}	V_{cn}	V_s
1	0	0	0	0	0	0	$V_0=0$
2	1	0	0	V_{dc}	0	0	$V_1=\frac{2}{3}V_{dc}$
3	1	1	0	V_{dc}	V_{dc}	0	$V_2=\frac{2}{3}V_{dc} \cdot e^{j(\pi/3)}$
4	0	1	0	0	V_{dc}	0	$V_3=\frac{2}{3}V_{dc} \cdot e^{j(2\pi/3)}$
5	0	1	1	0	V_{dc}	V_{dc}	$V_4=-\frac{2}{3}V_{dc}$
6	0	0	1	0	0	V_{dc}	$V_5=\frac{2}{3}V_{dc} \cdot e^{j(4\pi/3)}$
7	1	0	1	V_{dc}	0	V_{dc}	$V_6=\frac{2}{3}V_{dc} \cdot e^{j(5\pi/3)}$
8	1	1	1	V_{dc}	V_{dc}	V_{dc}	$V_7=0$

5.2. Modulation Techniques for Gating Signals

As can be seen from Table 5.1, the VSI produces only constant output voltage levels for various switching states. The inverter has to be controlled to compose desired voltage waveform by adjusting the voltage levels or space vectors as changing switching durations of switches so that the time average approximates the desired voltage reference. This control method is called modulation. The main purpose of the modulation is to acquire variable output having the highest fundamental component and the lowest harmonics [21]. There is some kind of modulation types and each has its own efficiency and total harmonic distortion ratio. The next section describes the most two

well-known modulation schemes for VSI.

5.2.1. Sinusoidal Pulse Width Modulation

Sinusoidal Pulse-Width Modulation (SPWM) is the modulation of PWM signal by comparing a sinusoidal (the carrier) wave with a saw tooth (the reference) wave by an analog comparator. Its advantages can be count as follows

- Easy to implement hardware
- Online operation
- Good power quality

Sinusoidal PWM techniques can be divided into two main types: bipolar SPWM and unipolar SPWM. In bipolar SPWM, the output voltage toggles between the negative and positive output voltages. In unipolar SPWM, the output voltage toggles between zero and the positive output voltage of the inverter. Figure 5.3 shows waveforms of the carrier, reference and output signals of bipolar SPWM.

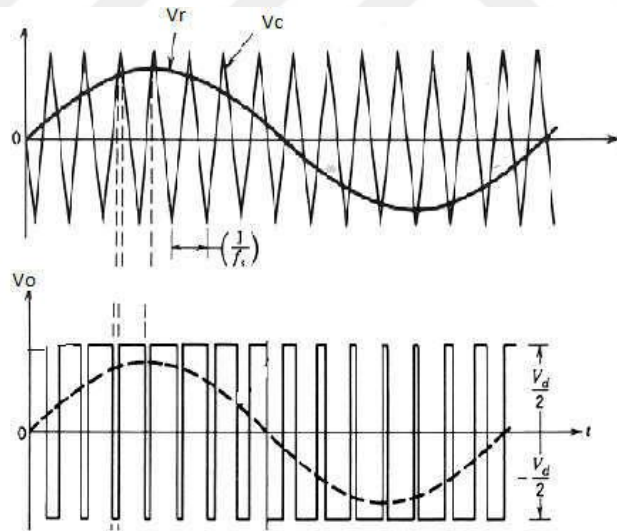


Figure 5.3 Signal forms of bipolar SPWM

5.2.2. Space Vector Pulse Width Modulation

Many studies show that Space Vector Pulse Width Modulation (SVPWM) has the most effective performance in terms of total harmonic distortion (THD) and current ripple among other methods. [18-21].

SVPWM technique is particularly the best method for the applications which have variable frequency drive with its intensive computation and advanced algorithm [22]. It is a modulation scheme used to apply a given voltage vector to a three-phase electric motor (e.g. PMSM or ACIM). The main purpose of SVPWM is emulating a frequency and amplitude adjustable three phase sinusoidal waveform by using a steady state DC voltage as changing the states of six switching components (e.g. MOSFETs and IGBTs). In order to better understand how SVPWM works, three phase inverter circuit can be simplified as shown in Figure 5.4.

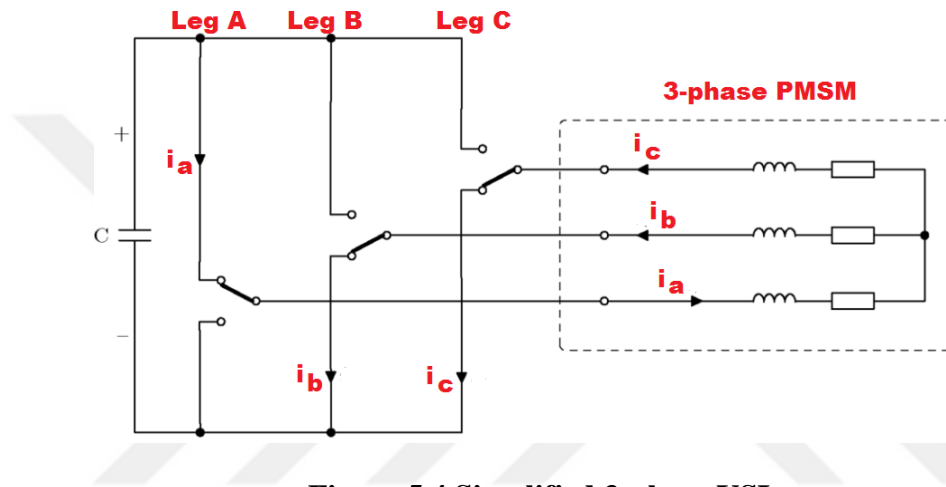


Figure 5.4 Simplified 3-phase VSI

As seen in Figure 5.4, one Single Pole Double Throw (SPDT) switch is used instead of two serial connected transistors for each individual leg. It can be assumed in this way because only one transistor in each bridge leg can be closed at any given time while the other transistor is open. In the figure above, there is one situation of eight ($2^3=8$) possible states. It shows that the upper transistor of leg A is closed (ON state), and upper transistors of leg B and leg C are open (OFF state). This situation can be defined as (1, 0, 0). Thus, the remaining six switching states give different voltages to the motor. These vectors, $\{0,0,1 \quad 0,1,0 \quad 0,1,1 \quad 1,0,0 \quad 1,0,1 \quad 1,1,0\}$, are called basic vectors, whereas two of them $\{0,0,0 \text{ and } 1,1,1\}$ always give zero voltage, called the zero vectors. Table 5.2 shows vector names and corresponding phases.

Table 5.2. Vectors and Corresponding Phases

Vector Name	Switch States (A,B,C)	Phase Vector
V_0	0,0,0	0
V_1	0,0,1	+C
V_2	0,1,0	+B
V_3	0,1,1	-A
V_4	1,0,0	+A
V_5	1,0,1	-B
V_6	1,1,0	-C
V_7	1,1,1	0

From Table 5.2, the phasor diagram of SVPWM can be drawn as in Figure 5.5. It must be stated that Phase A, Phase B, and Phase C are physical angles of stator windings, 120° apart from each other. Because each winding can have positive and negative voltages, that occupies two angles with a 180° -separation.

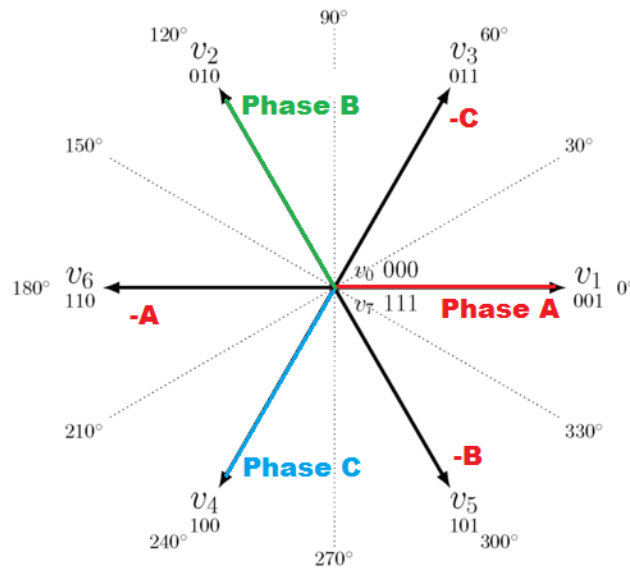


Figure 5.5 Space Vectors with their direction and magnitude

Now, any desired voltage vector can be generated by using two adjacent vectors with the suitable adjustment of magnitude of them. For instance, the reference vector is desired to be generated which can be seen in Figure 5.6.

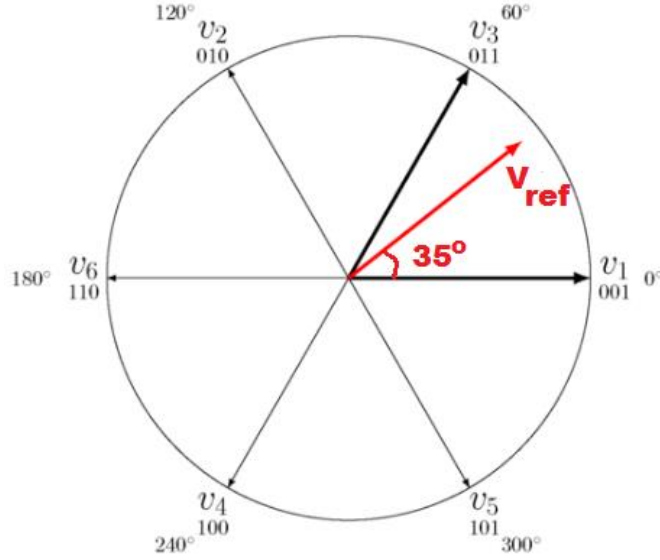


Figure 5.6 A sample reference vector to be emulated

As seen in Fig.5.6, a reference vector is placed between vectors V_1 and V_3 which is called sector 1. It is now possible to emulate this 35° reference vector with the resultant vector of magnitude adjusted V_1 and V_3 vectors. Note that the two zero vectors V_0 and V_7 are added to place dead time to the switching pattern. This dead time decreases the magnitude of the voltage and it is needed in conditions which the voltage reference magnitude is less than 100%.

In order to perform the SVPWM algorithm, the relationship between V_d - V_q voltage and line to neutral voltage (V_{an}, V_{bn}, V_{cn}) must be determined as seen in Fig. 5.6. Furthermore, Table 5.3 shows voltage vectors and corresponding line to neutral (V_{an}, V_{bn}, V_{cn}) and line to line voltages (V_{ab}, V_{bc}, V_{ca}). Note that the corresponding voltage must be multiplied by V_{dc} .

Table 5.3. Voltage Vectors and corresponding voltage

Vector Voltage	Switching Vectors			L-N Voltage			L-L Voltage		
	a	b	c	V _{an}	V _{bn}	V _{cn}	V _{ab}	V _{bc}	V _{ca}
V ₀	0	0	0	0	0	0	0	0	0
V ₁	1	0	0	2/3	-1/3	-1/3	1	0	-1
V ₂	1	1	0	1/3	1/3	-2/3	0	1	-1
V ₃	0	1	0	-1/3	2/3	-1/3	-1	1	0
V ₄	0	1	1	-2/3	1/3	1/3	-1	0	1
V ₅	0	0	1	-1/3	-1/3	2/3	0	-1	1
V ₆	1	0	1	1/3	-2/3	1/3	1	-1	0
V ₇	1	1	1	0	0	0	0	0	0

Firstly, by characterizing the relationships at the Table-3, the phase to phase voltage and phase to neutral voltage can be arranged in matrix form as follow, respectively

$$\begin{bmatrix} V_{ab} \\ V_{bc} \\ V_{ca} \end{bmatrix} = V_{dc} \cdot \begin{bmatrix} 1 & -1 & 0 \\ 0 & 1 & -1 \\ -1 & 0 & 1 \end{bmatrix} \cdot \begin{bmatrix} a \\ b \\ c \end{bmatrix} \quad (5.1)$$

$$\begin{bmatrix} V_{an} \\ V_{bn} \\ V_{cn} \end{bmatrix} = \frac{V_{dc}}{3} \cdot \begin{bmatrix} 2 & -1 & -1 \\ -1 & 2 & -1 \\ -1 & -1 & 2 \end{bmatrix} \cdot \begin{bmatrix} a \\ b \\ c \end{bmatrix} \quad (5.2)$$

5.2.3. SVPWM technique

The SVPWM technique can be summarized by the following three main steps [23]:

Step 1: Determination of V_d, V_q, V_{ref}, and angle (α)

As can be seen in Figure 5.7, V_d and V_q can be calculated in terms of line voltages

$$\begin{aligned} V_d &= V_{an} - V_{bn} \cdot \cos 60^\circ - V_{cn} \cdot \cos 60^\circ \\ V_d &= V_{an} - \frac{1}{2} V_{bn} - \frac{1}{2} V_{cn} \end{aligned} \quad (5.3)$$

$$V_q = 0 + V_{bn} \cdot \cos 30^\circ - V_{cn} \cdot \cos 30^\circ \quad (5.4)$$

$$V_q = \frac{\sqrt{3}}{2} V_{bn} - \frac{\sqrt{3}}{2} V_{cn}$$

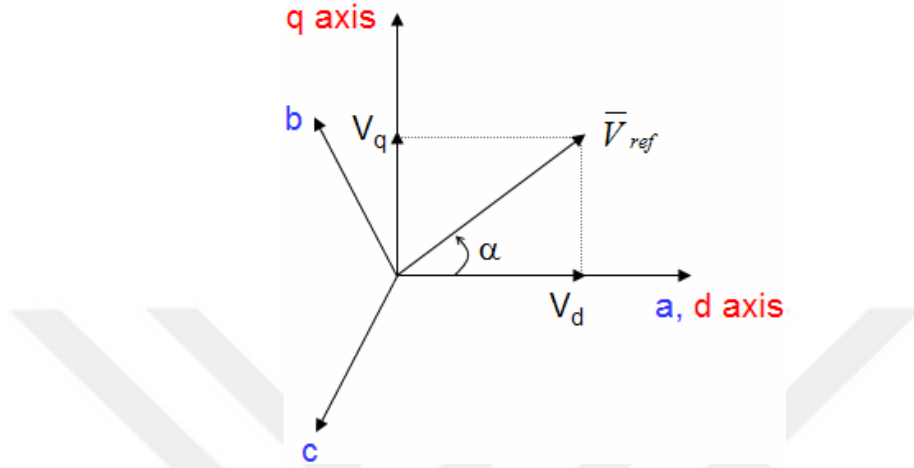


Figure 5.7 Reference Voltage and its component in dq axis

From Eq. (5.3) and (5.4) V_d and V_q could be arranged in matrix from

$$\begin{bmatrix} V_d \\ V_q \end{bmatrix} = \frac{2}{3} \cdot \begin{bmatrix} 1 & -\frac{1}{2} & -\frac{1}{2} \\ 0 & \frac{\sqrt{3}}{2} & -\frac{\sqrt{3}}{2} \end{bmatrix} \cdot \begin{bmatrix} V_{an} \\ V_{bn} \\ V_{cn} \end{bmatrix} \quad (5.5)$$

The magnitude of the reference voltage vector (V_{ref}) is calculated by Pythagoras' Theorem

$$|\overrightarrow{V_{ref}}| = \sqrt{V_d^2 + V_q^2} \quad (5.6)$$

The angle (α) can be calculated by

$$\alpha = \tan^{-1} \left(\frac{V_q}{V_d} \right) \quad (5.6)$$

Step 2: Determination of the time durations T_1 , T_2 and T_0

The reference voltage vector can be represented with two adjacent vectors. For

instance, as seen in Figure 5.8, the reference voltage vector is at sector 1.

It means that the reference vector can be constructed by the fine-tuned magnitudes of V_1 , V_2 , and zero vectors.

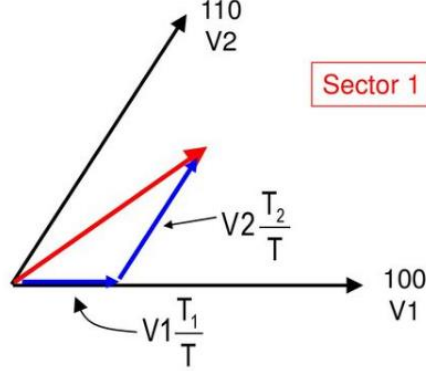


Figure 5.8 Two adjacent vectors composing the reference vector

In Figure 5.7, T is sampling period, V_1 vector is applied for T_1 duration, V_2 vector is applied for T_2 duration and the zero vector is applied for the rest of sampling period T . The zero vector can be defined as

$$T_0 = T - T_1 - T_2 \quad (5.7)$$

Switching duration for sector 1, can be calculated as

$$\int_0^T \overline{V_{ref}} dt = \int_0^{T_1} \overline{V_1} dt + \int_{T_1}^{T_1+T_2} \overline{V_2} dt + \int_{T_1+T_2}^T \overline{V_0} dt \quad (5.8)$$

$$T \cdot \overline{V_{ref}} = (T_1 \cdot \overline{V_1} + T_2 \cdot \overline{V_2}) \quad (5.9)$$

$$T \cdot |V_{ref}| \cdot \begin{bmatrix} \cos(\alpha) \\ \sin(\alpha) \end{bmatrix} = T_1 \cdot \frac{2}{3} V_{dc} \begin{bmatrix} 1 \\ 0 \end{bmatrix} + T_2 \cdot \frac{2}{3} V_{dc} \begin{bmatrix} \cos(\pi/3) \\ \sin(\pi/3) \end{bmatrix} \quad (5.10)$$

where $0 \leq \alpha \leq 60^\circ$

$$T_1 = T \cdot a \cdot \frac{\sin(\frac{\pi}{3} - \alpha)}{\sin(\pi/3)} \quad (5.11)$$

$$T_2 = T \cdot a \cdot \frac{\sin(\alpha)}{\sin(\pi/3)} \quad (5.12)$$

$$T_0 = T - T_1 - T_2 \quad (5.7)$$

$$T = \frac{1}{f} \quad (5.13)$$

Finally modulation index (a) can be calculated

$$a = \frac{|V_{ref}|}{\frac{2}{3}V_{dc}} \quad (5.14)$$

The switching time durations T1, T2 and T0 of any given sector can be calculated by

$$\begin{aligned} T_1 &= \frac{\sqrt{3} \cdot T \cdot |V_{ref}|}{V_{dc}} \left(\sin \left(\frac{\pi}{3} - \alpha + \frac{n-1}{3} \pi \right) \right) = \frac{\sqrt{3} \cdot T \cdot |V_{ref}|}{V_{dc}} \left(\sin \frac{n}{3} \pi - a \right) \\ &= \frac{\sqrt{3} \cdot T \cdot |V_{ref}|}{V_{dc}} \left(\sin \frac{n}{3} \pi \cdot \cos \alpha - \cos \frac{n}{3} \pi \cdot \sin \alpha \right) \end{aligned} \quad (5.15)$$

$$\begin{aligned} T_2 &= \frac{\sqrt{3} \cdot T \cdot |V_{ref}|}{V_{dc}} \left(\sin \left(\alpha - \frac{n-1}{3} \pi \right) \right) \\ &= \frac{\sqrt{3} \cdot T \cdot |V_{ref}|}{V_{dc}} \left(-\cos \alpha \cdot \sin \frac{n-1}{3} \pi + \sin \alpha \cdot \cos \frac{n-1}{3} \pi \right) \end{aligned} \quad (5.16)$$

Step 3: Determination the transistor's (S₁ to S₆) switching time

Switching times of the three upper transistors of VSI for any given sector is illustrated in Figure 5.9 [25]. Based on this layout, Table 5.4 summarizes the calculations of switching times.

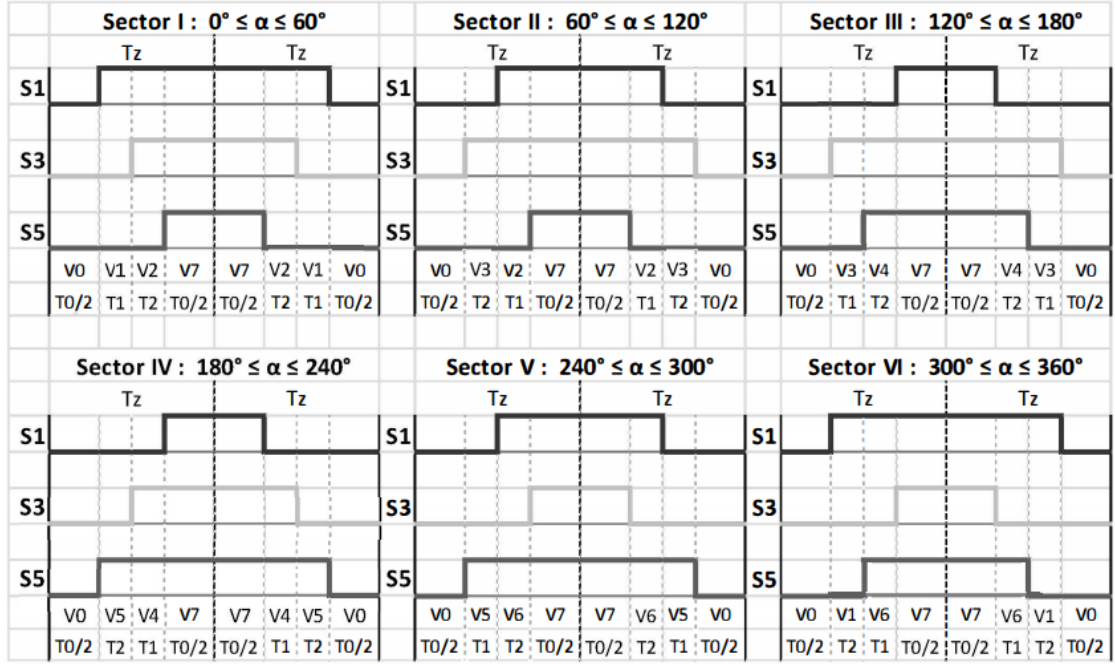


Figure 5.9 Switching patterns and corresponding switching time durations [25]

As seen in Figure 5.8, the switching period T is divided into two symmetrical parts by the symmetric 7-segment technique. It is shown that the sequence $V_0 - V_1 - V_2 - V_0$ is used in the first $T/2$, and the sequence $V_0 - V_2 - V_2 - V_0$ is used in the second $T/2$. The sequences are symmetrical [26]. This technique is generally preferred due to its total harmonic distortion (THD) performance [27].

Table 5.4. Switching calculations of upper and lower transistors for all sectors

Sector	Upper IGBT Groups (S_1, S_3, S_5)	Lower IGBT Groups (S_4, S_6, S_2)
1	$S_1 = T_1 + T_2 + T_0/2$ $S_3 = T_2 + T_0/2$ $S_5 = T_0/2$	$S_4 = T_0/2$ $S_6 = T_1 + T_0/2$ $S_2 = T_1 + T_2 + T_0/2$
2	$S_1 = T_1 + T_0/2$ $S_3 = T_1 + T_2 + T_0/2$ $S_5 = T_0/2$	$S_4 = T_2 + T_0/2$ $S_6 = T_0/2$ $S_2 = T_1 + T_2 + T_0/2$
3	$S_1 = T_0/2$ $S_3 = T_1 + T_2 + T_0/2$ $S_5 = T_2 + T_0/2$	$S_4 = T_1 + T_2 + T_0/2$ $S_6 = T_0/2$ $S_2 = T_1 + T_0/2$
4	$S_1 = T_0/2$ $S_3 = T_1 + T_0/2$ $S_5 = T_1 + T_2 + T_0/2$	$S_4 = T_1 + T_2 + T_0/2$ $S_6 = T_2 + T_0/2$ $S_2 = T_0/2$
5	$S_1 = T_2 + T_0/2$ $S_3 = T_0/2$ $S_5 = T_1 + T_2 + T_0/2$	$S_4 = T_1 + T_0/2$ $S_6 = T_1 + T_2 + T_0/2$ $S_2 = T_0/2$
6	$S_1 = T_1 + T_2 + T_0/2$ $S_3 = T_0/2$ $S_5 = T_1 + T_0/2$	$S_4 = T_0/2$ $S_6 = T_1 + T_2 + T_0/2$ $S_2 = T_2 + T_0/2$

Finally, it can be emphasized that SVPWM technology has advantages over SPWM such as reduced harmonic content, switching losses, and higher DC voltage utilization rate [28].

6. PMSM DRIVE WITH SENSORLESS CONTROL

In this chapter, a sensorless PMSM drive approach is introduced. For PM machine drives, vector control techniques have become very popular because they provide one of the best performances over conventional ones. A vector-based control eliminates almost all the disadvantages of scalar control. Furthermore, it is easier to implement the hardware of vector control. The basic requirement of this approach is to control the magnitudes and angles of space vectors. For specifications with the desired high performance and constant torque dynamics, vector control appears to be the most appropriate control method [28].

FOC is an important variant of vector control methods. The objective of the FOC is to control the magnetic flux and the torque by regulating the d and q components of the stator currents or relatively fluxes. With the knowledge of stator currents and rotor flux position, the torque and the flux of the motor can be controlled very effectively by the FOC. Apart from many advantages, the fast response and small torque fluctuation are the main advantages of the FOC. The realization of this technique is mostly performed by using three current controllers. These are for the direct-axis component, the quadrature-axis component and the speed, respectively [29]. These regulators are generally selected as PI controllers. Besides, in this study, a new control scheme based on the power function called Power Based Controller (PBC) will be introduced as an alternative to PI control.

6.1. FOC Scheme

Field-Oriented Control is the technique used to achieve the decoupled (decomposed) torque and flux control by converting stator current quantities (phase currents) in the fixed reference frame into torque and flux generating current components in the rotating reference frame. The advantages of FOC are [30].

- Transformation of a complex and coupled AC model into a simple linear model
- Independent torque and flux control similar to DC motor
- Fast dynamic response and good transient and steady-state performance
- High torque and low current at startup

- High Efficiency
- Wide speed range through field weakening

The block diagram of the FOC is shown in Figure 6.1. Since all transformations in the blocks and the SVPWM technique are introduced in the previous sections, they will not be included here.

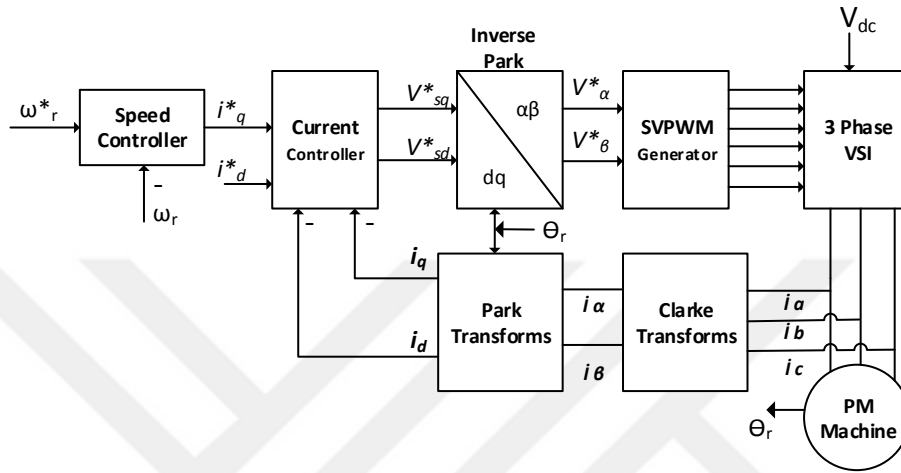


Figure 6.1 Block Diagram of FOC

From Figure 6.1, it can be seen that, Park and Inverse Park Transformation blocks require the rotor position or angle information together with the two phase currents and voltages. For a PMSM, the rotor flux angle Θ_r is the same with position of the rotor. The FOC scheme equipped with sensors provides the shaft position for almost all range of speed. In the sensorless FOC scheme, the angle Θ_r must be estimated by a current observer [16]. These two methods are explained in the following sections.

The implementation of sensorless FOC algorithm can be defined step by step as [31].

1. The 3-phase stator currents i_a , i_b and i_c are measured. i_c can be also calculated by the Kirchoff's Current Law ($i_a + i_b + i_c = 0$) without measurement.
2. The CT is applied to the 3-phase currents (i_a , i_b and i_c). This results in two new orthogonal currents (i_α and i_β) in two-axis stationary coordinate system. Thus, the transformation provides the variables i_α and i_β using the measured quantities i_a , i_b and the calculated quantity i_c . Now, i_α and i_β are time-dependent quadrature current vectors from a stator perspective.

3. The PT is applied to the orthogonal current vectors (i_α and i_β) and it provides two rotating current vectors (I_d and I_q) in a two-axis rotating coordinate system aligned with the rotor flux. I_d and I_q become constant while steady-state condition takes place. This means that these currents become DC quantities after the transformation is complete.
4. Closed loop control is applied to I_d and I_q currents. The references of I_d and I_q currents regulate rotor magnetizing flux and torque output, respectively. The output of the controllers will yield the voltage vectors of V_d and V_q , as the input voltages for VSI after applying IPT.
5. The position estimator using the inputs of V_α , V_β , I_α and, I_β , estimates a transformation angle. This new angle leads the FOC scheme to determine the location of the next voltage vector.
6. By applying IPT, each output of the current controllers of V_d and V_q are transformed back to the two-axis stationary coordinate using the estimated angle. V_α and V_β voltage vectors are determined after this transformation.
7. The V_α and V_β voltages are converted to three-phase values of V_a , V_b , and V_c . These voltages are used to specify the next PWM duty cycle, achieving the required vector.

All transformations, of current regulators, iteration, and SVPWM generator is illustrated in Figure 6.1.

To perform an FOC algorithm, the motor position must be continuously determined. This is one of the most important steps of the algorithm. There are two main methods of how to calculate the commutation angle required for the FOC. These are methods with and without sensors. The next two sections summarize these methods. Since the sensorless method are used in this study, the other method is briefly introduced.

6.2. Position Detection Methods in FOC

To implement the FOC algorithm, it is essential to determine the angle of the rotor flux position using certain methods. The conventional method uses position sensors such as Hall Effect Sensors, quadrature encoders or resolvers. However, for

crucial reasons such as cost and robustness, it may not be a good option to install additional sensors in the motor [15]. Thus, in recent years, sensorless techniques have been replaced with sensorized ones. The following sections introduce these two methods.

6.2.1. Sensored Method

The sensor-based techniques utilize electromechanical devices assembled to the rotor to acquire the position and the speed of the rotor. Most commonly used position detection devices are resolvers, encoders, and hall-effect sensors.

Among the three sensor types, Hall Effect sensors are considered to be the most cost-effective and most common detection method.

The three Hall Effect sensors ensure data for every 60° advance in the position of the rotor, providing exact timing for motor commutations. Applications, where accurate location detection is important, the best sensor topology is resolver. Although resolver technology has the best precise position detection performance, it costs more than the other two because it is mounted externally to the motor.

The resolution of optical incremental encoders is still high. However, they are not enough to feel the absolute position at power-up. In addition, the optical encoder is expensive because it is externally mounted. Figure 6.2 illustrates the sensor output waveforms for all three sensor types.

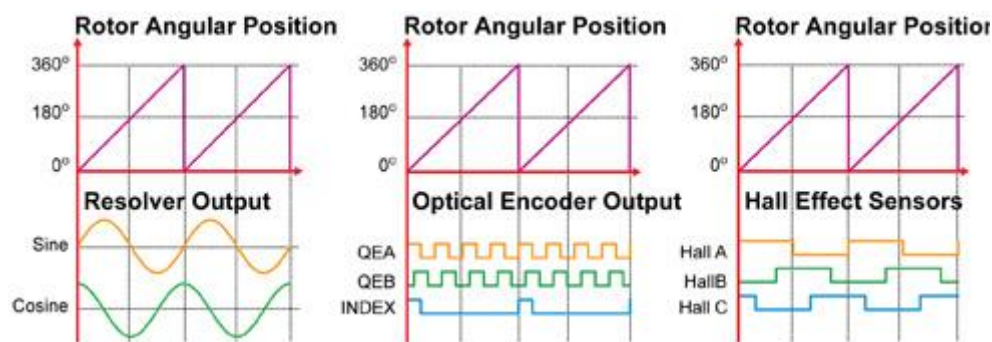


Figure 6.2 Sensor Outputs of the Position Sensor Types

6.2.2 Sensorless Method

The position calculation technique based on sensorless operation performs the FOC algorithm by estimating the position of the motor. There are many methods and

classification of sensorless position detection techniques in PMSM drives. Figure 6.3 shows a detailed classification of sensorless position detection methods [32].

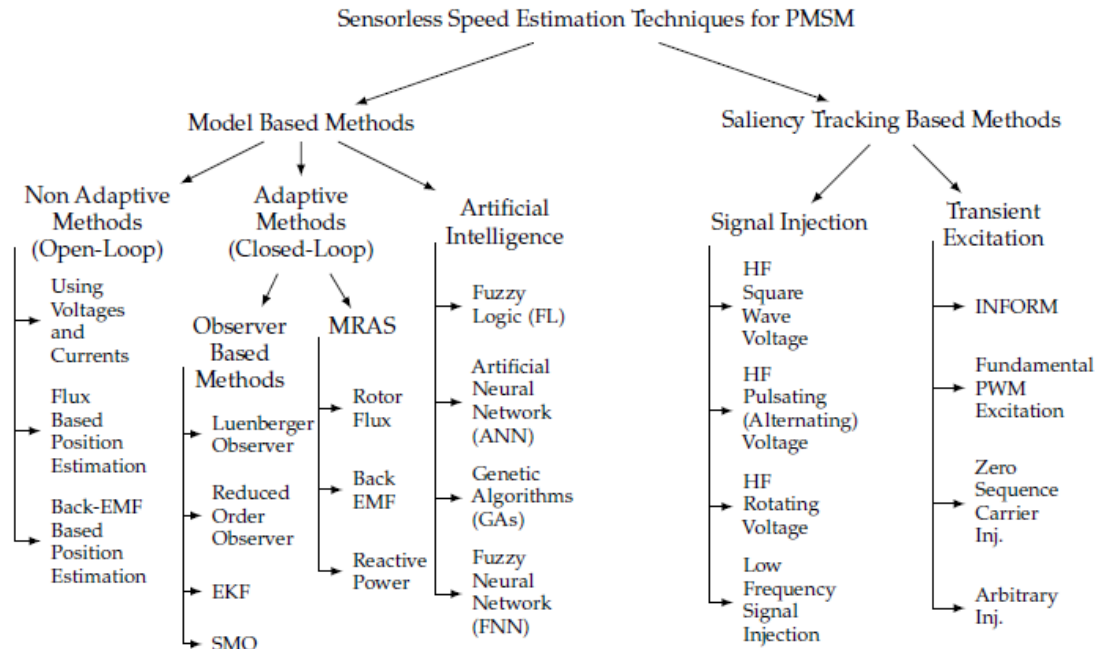


Figure 6.3 Classification of sensorless position detection methods for PMSM drive [32]

As shown in Figure 6.3, sensorless position detection methods are divided into two main groups:

1. Model-based methods
2. Saliency and signal injection methods.

Model-based methods do not offer efficient performance at zero or low speed due to initial rotor position error, stator current, and voltage measurement errors, inverter, and machine linearity. Furthermore, because the model-based methods depend on the back EMF voltage proportional to the rotor speed, these techniques fail at zero and low-speed regions. However, model-based sensorless methods provide good performance for medium and high-speed regions. Saliency and signal injection techniques can provide good results at zero or low speeds because they do not require back EMF voltage. However, these techniques have major drawbacks such as audible noise, torque fluctuations, and vibration [32].

6.3. Position Estimator Based on Sliding Mode Current Observer

One of the model-based techniques, the Sliding Mode Observer (SMO) is preferred for estimating the position in the experimental setup of this thesis because of its various advantages such as having a simple structure, robustness, fast application time and being free from motor parameters. The problem of zero and low speed is tried to be overcome by using an open-loop flux-based estimator from the start-up to a certain speed level. Among the various techniques, SMO stands out for its robustness of measurement noise, parameter deviations and an inherent high-gain structure. [33].

The general block diagram of rotor flux position estimator based on the SMCO is shown in Figure 6.4. The inputs to the estimator are motor phase currents and voltages expressed in a $\alpha\beta$ coordinate frame.

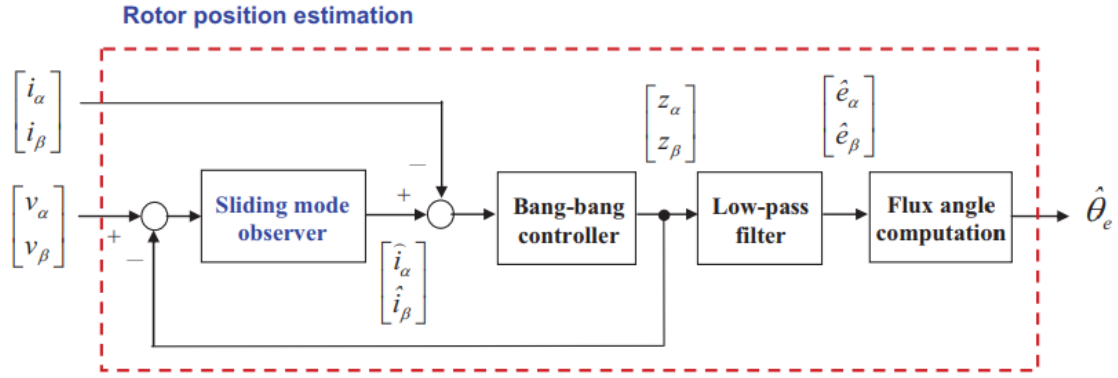


Figure 6.4 Rotor flux position estimator based on SMO [34]

The SMO based back EMF estimator consists of a model-based current observer and a digital positioner. The positioner is driven by error between estimated motor currents and actual motor currents. The mathematical equation for the observer and positioner is given by, respectively [35].

$$\frac{d}{dt} \cdot \hat{i}_s = A \cdot \hat{i}_s + B(v_s^* - \hat{e}_s - z) \quad (6.1)$$

$$z = k \cdot \text{sign}(\hat{i}_s - i_s) \quad (6.2)$$

The positioner called bang-bang control z is used to drive the current estimation

error to zero. This is achieved by selecting a proper value for sliding mode gain k and correct formation of estimated BEMF, \hat{e}_s . The accent symbol (^) represents the estimated variables and the symbol (*) represents the command variable. Writing Eq. (6.1) and (6.2) in discrete form by,

$$\hat{i}_s(n+1) = F \cdot \hat{i}_s(n) + G(v_s(n)^* - \hat{e}_s(n) - z(n)) \quad (6.3)$$

$$z(n) = k \cdot \text{sign}(\hat{i}_s(n) - i_s(n)) \quad (6.4)$$

where $\hat{i}_s(n) - i_s(n)$ is current error and can be notated as $\tilde{i}_s(n)$.

The matrices F and G represent discrete mathematical model and are given by, respectively

$$F = \exp^{-\frac{R}{L}T_s} \cdot I_2 \quad (6.5)$$

$$G = \frac{1}{R} (1 - \exp^{-\frac{R}{L}T_s}) \cdot I_2 \quad (6.5)$$

where T_s is sampling time and I_2 is a 2×2 identity matrix.

The estimated BEMF is obtained by filtering the output of bang-bang control (z), by using a first order low pass filter, can be defined as

$$\frac{d}{dt} \cdot \hat{e}_s(n+1) = -\omega_0 \cdot \hat{e}_s(n) + \omega_0 \cdot z \quad (6.6)$$

The parameter ω_0 is defined as

$$\omega_0 = 2\pi f_0 \quad (6.7)$$

where f_0 represents the cutoff frequency of the filter in cycles /sample and is given by

$$f_0 = \frac{f_o}{f_s} \quad (6.8)$$

where f_o is cut-off frequency in cycles/sec and f_s is sampling frequency in samples/sec.

Eq (6.6) can also be written in discrete form by

$$\hat{e}_s(n+1) = \hat{e}_s(n) + 2\pi f_0(z(n) - \hat{e}_s(n)) \quad (6.9)$$

Finally, the estimated rotor flux angle is obtained as

$$\hat{\theta}_s = \tan^{-1}\left(-\frac{\hat{e}_{s\alpha}}{\hat{e}_{s\beta}}\right) \quad (6.10)$$

Estimated speed can be calculated by taking derivative of the estimated angle above, with respect to time.

The algorithm of the rotor flux position estimator based on SMCO can be summarized as follow [34]:

Step 1: Read the values $i_{s\alpha}(n), i_{s\beta}(n), v_{s\alpha}(n), v_{s\beta}(n)$ in $\alpha\beta$ axis.

Step 2: Estimate the estimated current ($\hat{i}_{s\alpha}, \hat{i}_{s\beta}$) by using Eq.(6.3)

Step 3: Calculate the current error by

$$\begin{aligned} \tilde{i}_{s\alpha}(n) &= \hat{i}_{s\alpha}(n) - i_{s\alpha}(n) \\ \tilde{i}_{s\beta}(n) &= \hat{i}_{s\beta}(n) - i_{s\beta}(n) \end{aligned} \quad (6.11)$$

Step 4: Obtain the z gain of the current observer by using Eq (6.4)

Step 5: Estimate the BEMF by using Eq. (6.6)

Step 6: Obtain the estimated rotor position by using Eq. (6.10)

Then set $n = n+1$ and back to **Step 1**

6.4. Speed and Current Control Loops

In a classical FOC structure, there are generally three regulators to control three inputs independently. These are speed controller, direct current (i_d) and quadrature current (i_q) controllers as shown in Figure 6.5.

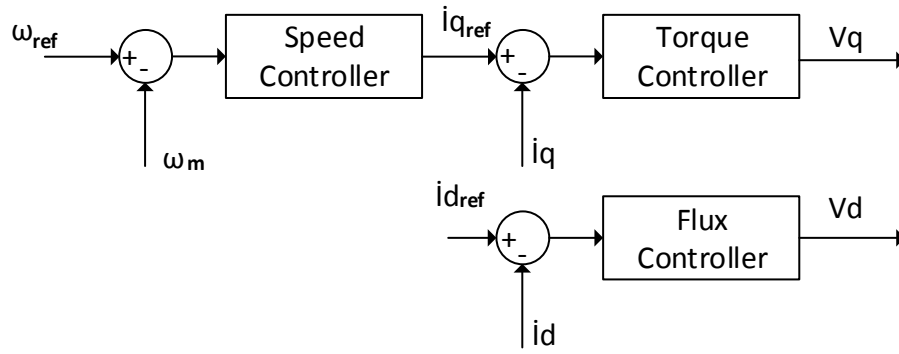


Figure 6.5 Control Loops in FOC

The direct (magnetizing) current (i_d) denotes the field current responsible for the magnetic field and the quadrature current (i_q) denotes the armature current responsible for the torque. The currents i_d and i_q are aligned orthogonally so that, the field component is unaffected or constant when controlling the torque component. Since i_q provides useful torque, and i_d has no positive contribution to torque generation, the reference direct axis current i_{d_ref} for the PMSM motor is considered zero. Therefore, the current space vector is forced in a quadratic direction, so that a maximum torque can be achieved [36].

As can be seen from Figure 6.5, the reference torque for quadrature current feedback is a function of the speed error. The speed error between the reference and actual value of speed is amplified by the speed controller to cancel the error and to generate a reference torque (i_{qref}). The main object of the speed controller is to minimize the speed error by controlling the electromagnetic torque [37].

To control these three quantities (speed, torque, and flux), PI controllers are often used in the FOC algorithm because they are easy to implement, robust and provide good dynamic results when tuning properly. In this thesis, a new control scheme, called Power Function-Based Controller (PBC) is used for similar purposes.

6.4.1. PI controller

A typical PI controller comprises proportional and integrative components, as shown in the block diagram in Figure 6.6.

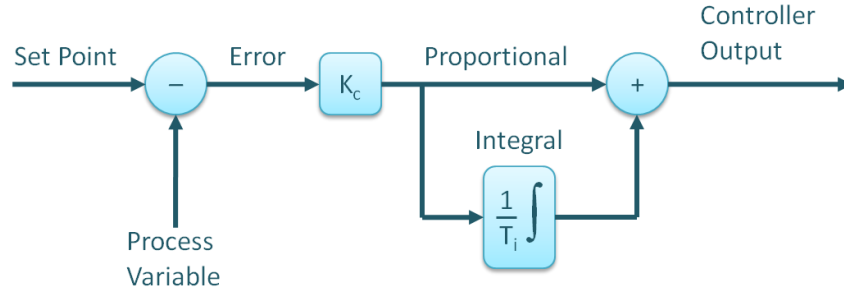


Figure 6.6 PI controller block diagram

The mathematical model of a PI controller is stated in the continuous-time domain as

$$C_o = C_{ob} + K_c e(t) + K_c \cdot \frac{1}{T_i} \int e(t) \cdot dt \quad (6.12)$$

Where C_o , C_{ob} , K_c , T_i , and $e(t)$ are the controller output, controller bias, controller gain, reset time, and error difference between the set-point and the process variable, respectively.

6.4.2. Power function based controller (PBC)

The proposed control scheme basically can be characterized by a power function of Kx^λ where K , x and λ are the gain, base (feedback error), and exponent, respectively. As can be seen, the control scheme shows both linear and nonlinear properties relative to the λ . A power function can generate a real or complex number depending on its base and exponent. In this study, for the speed and torque control, the PBC is considered scalar like a PI because of performing the control action under dq -axis rotating reference frame, i.e., no phase variation. In order for the power function to yield a scalar or real part only, the necessary and sufficient condition is that either only the base must be positive real (first case) or it must be negative real with an integer exponent (second case). The second case ($x < 0.0$) restricts λ to take only integer values. In addition, the power function generates positive and negative real values for even and odd integer values λ , respectively. However, in terms of control, the goal for this last case should generate a negative real value for any real value of λ . To overcome this challenge and allow λ to take any real value, a reasonable arrangement for the control scheme, yielding a symmetrical output, can be suggested as

$$u_{pf} = \begin{cases} K(e_r)^\lambda & e_r \geq 0 \\ -K|e_r|^\lambda & e_r < 0 \end{cases} \quad (6.13)$$

Where u_{pf} and e_r are the power function controller output and feedback error, respectively.

Because of symmetrical oscillation of the output around the set point, the gain K can be remained unchanged regardless of the error. Hence, the control scheme can be reduced to a single-line source code using signum function

$$u_{pf} = K \frac{e_r}{|e_r| + \varepsilon} |e_r|^\lambda \quad (6.14)$$

Where ε is a softening factor and also prevents the zero division error.

Figures 6.7 and Figure 6.8 use the error-exponent-gain data to realize better the behavior of the controller. Figure 6.7 shows the variation of the controller output with respect to the exponent for different error values at a constant gain. Figure 6.7 shows the controller varying with respect to the lambda may exhibit linear or non-linear behavior for different error values. This means that the controller can be effective in linear and nonlinear systems.

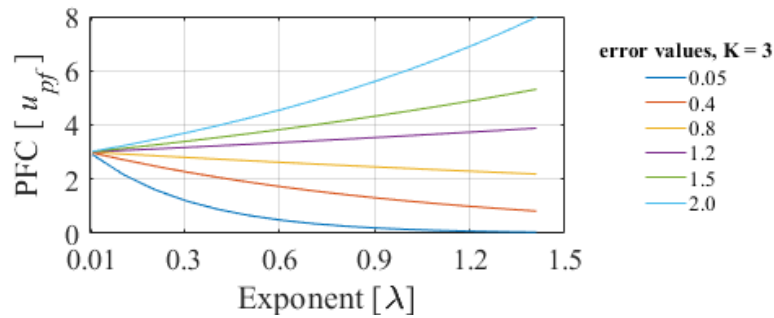


Figure 6.7 Variation in exponent for different error values at a constant gain

It appears that K does not alter the controller behavior, just the amplitude of the controller. Figure 6.8 shows that the controller output changes non-linearly with respect to the error. It is seen that the rate of change of the output can be changed by gain. It is seen in Figure 6.8 that the controller output becomes symmetrical according to the

negative and positive error variations with the arrangement made in the controller.

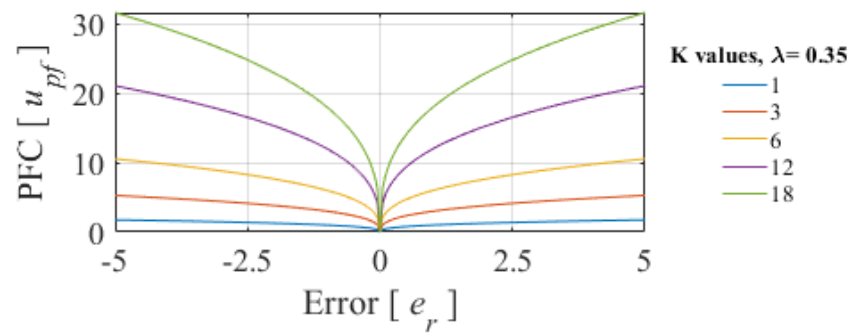


Figure 6.8 Variation in the error with different gain values at constant λ

7. SIMULATION STUDY

All modeling and simulations are performed in MATLAB/Simulink environment. The aim is to model the PMSM which is used in WMs and simulate a suitable PMSM driver which is based on FOC algorithm. As stated in the previous chapters, there are generally three PI controllers in a classical FOC drive to regulate the speed and currents. In this thesis, a new controller design, PBC is also simulated in order to compare its performance with respect to PI controllers.

The first step of simulation study is modeling PMSM. Before starting to model a machine, its vital parameters must be known. Table 7.1 shows important parameters of PMSM which is modeled in this study.

Table 7.1 PMSM Parameters

Item	Quantity
Stator Resistance (R)	3.15 Ω
Inductance (Lq)	18mH
Inductance (Ld)	16mH
Rotor Flux Constant (ψ)	0.1546V/rad/s
Moment of Inertia (J)	0.00176kgm ²
Friction Viscous Gain (B)	0.0004Nm/rad/s
Number of Pole Pairs	4
Motor Power (W)	950W

PMSM can be modeled in different reference frames which are introduced in details at Chapter 6. In this thesis, dq coordinate (rotating reference frame) model of PMSM is preferred due to time-independency. Figure 7.1 shows Simulink schematic of modeled PMSM. As seen Figure 7.1, PMSM model block are constructed by three sub-block. They have also lower level blocks which are grouped into makeable blocks. Some of the lower level blocks can be seen in the Appendix A.

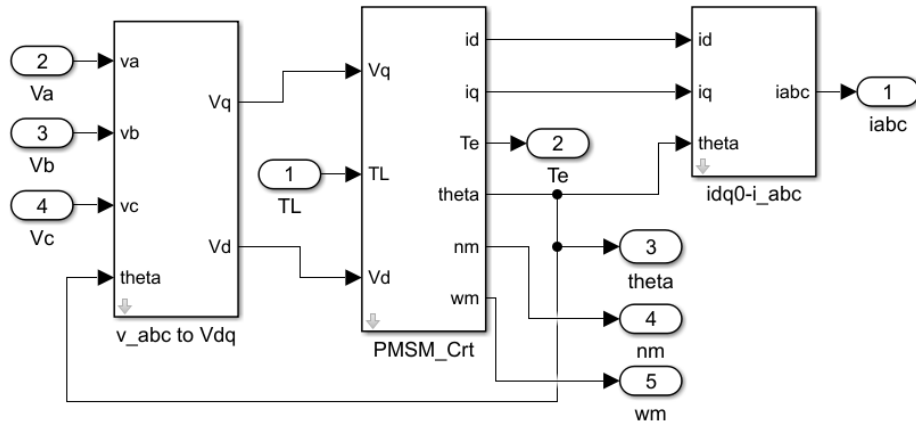


Figure 7.1 Simulink Schematic of modeled PMSM

General scheme of the studied PMSM drive scheme is shown in Figure 7.2. There are two parallel simulations which both is based FOC but differs in controller types. While right-hand side of the simulation is having PI regulators for speed and current controlling, left-hand side has a new regulator which is called PCB. The simulation is held in this way in order to obtain simultaneous results. Furthermore, IPT and SVPWM blocks, which can be seen at the Appendix, are embedded into controller block in order to reduce complexity of simulation scheme. Similarly, for the simplicity, angle information which is necessary for PT and IPT blocks, comes from PMSM model itself, instead of adding position estimator blocks to the simulation scheme.

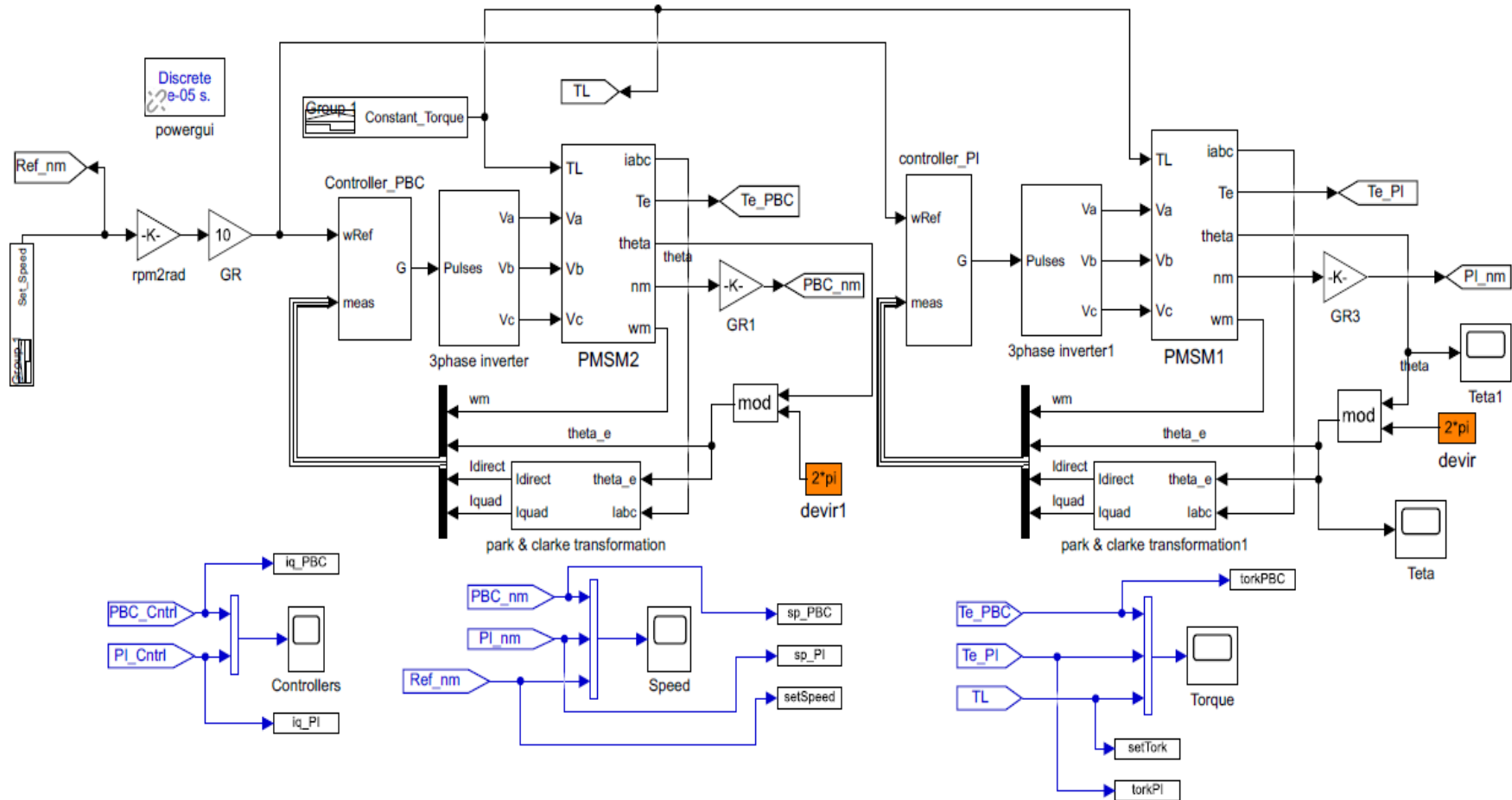


Figure 7.2 Comparative Simulation Study Overview

Simulations are conducted under two main configurations depends on the reference load torque, which is shown in Table 7.2.

Table 7.2 Simulation Cases

CASE	TORQUE TYPE
Case 1	Constant Load Torque (Toggles 10Nm to 2Nm)
Case 2	Variable Load Torque (Alternates between 10Nm to 2Nm)

In the first case, as seen in Figure 7.3, a constant load torque signal which starts with 10Nm and ends with 2Nm is applied to PMSM and results are observed. In the second case, a variable load torque signal which alternates between 10Nm and 2Nm, as seen in Figure 7.4, is applied to the PMSM.

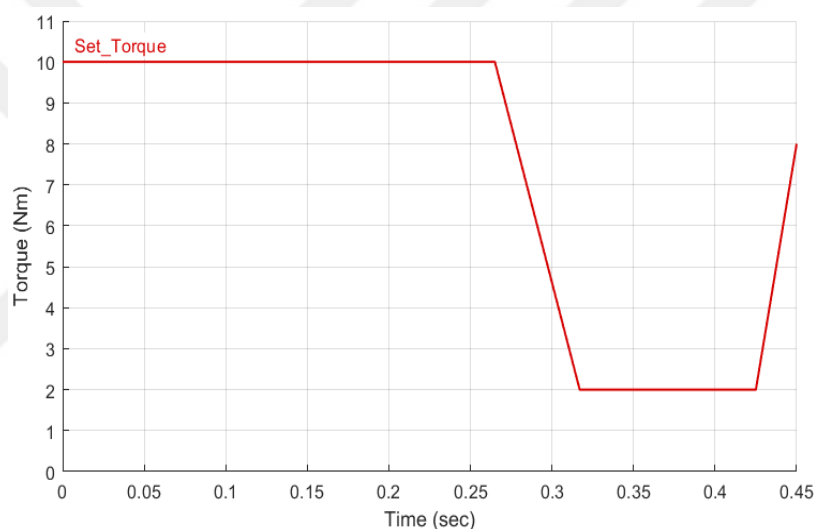


Figure 7.3 Constant Torque applied to the PMSM

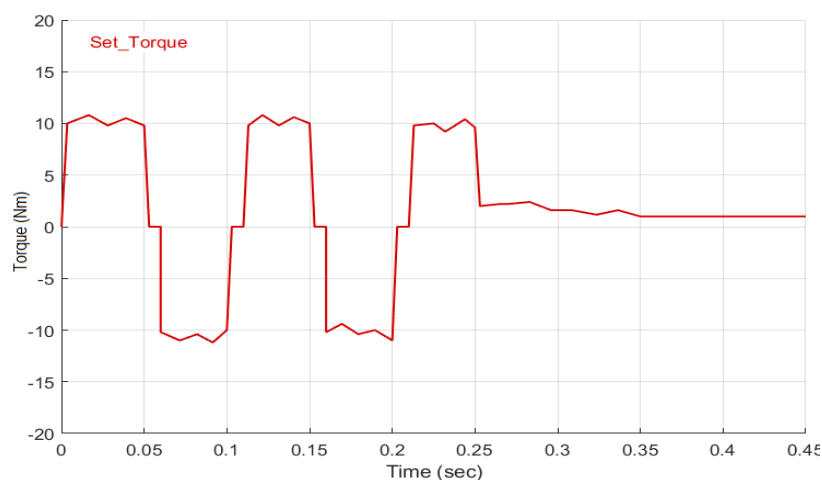


Figure 7.4 Variable Torque Load applied to the system

However, both case is conducted for the same reference speed signal which is shown in Figure 7.5. It is composed in such a way that it can represent washing and spinning-drying cycles of WM operation, which is introduced in chapter 2. After it alternates between 100RPM and -100RPM in washing cycle, the reference speed is then increasing up to 800RPM in which spinning-drying cycle is emulated. Note that the minus (-) RPM represents reversal motion of PMSM.

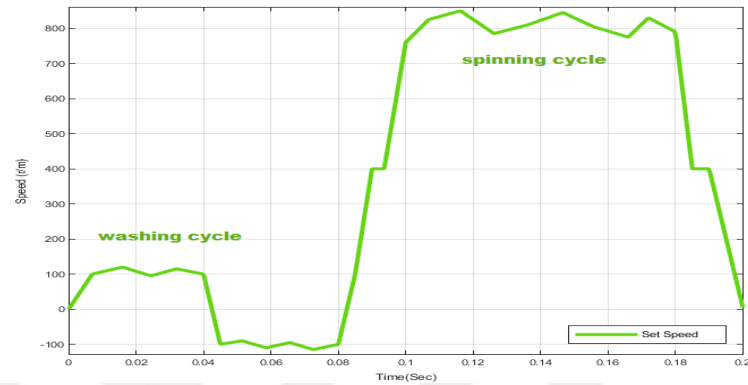


Figure 7.5 The Reference Speed

For the case 1, simulation result for the speed control is shown in Figure 7.6. It is clearly seen that PI controller and PBC controller has nearly the same performance. Since PI controller has slightly bigger overshoot than PBC has, it can be evaluated as PBC is better than PI at speed control.

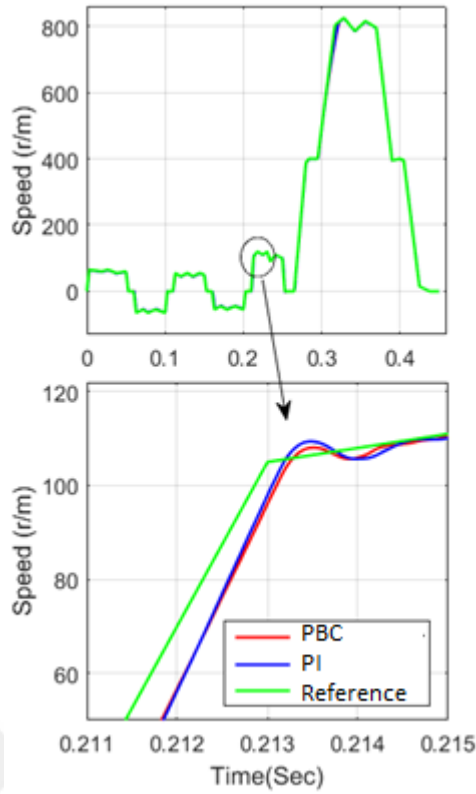


Figure 7.6 Comparative simulation results for the speed control for case 1

In the first case, a constant 10Nm load torque is applied to the PMSM while its speed travels in -100 and 100 RPM. After PMSM's speed reaches at 800RPM, the applied torque is decreased to 2Nm as shown in Figure 7.3. Torque controllers results are shown in Figure 7.7. According to graphic, PI Controller and PBC controller is showing the exact same performance.

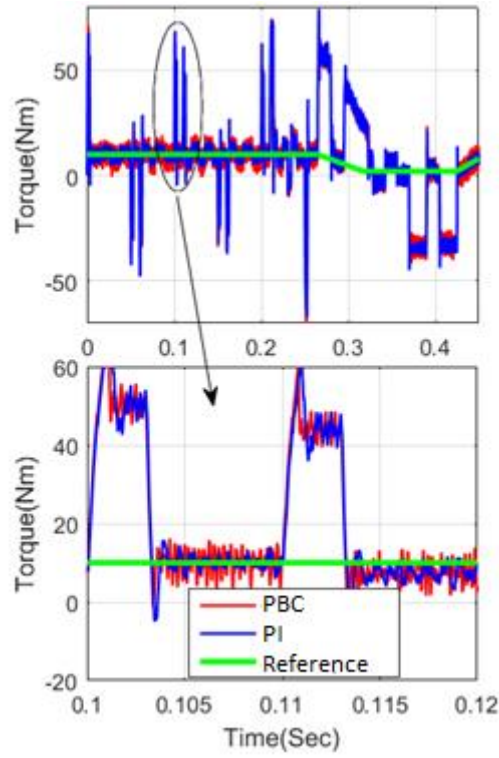


Figure 7.7 Comparative simulation results of the torque control for the case 1

Finally, for the case 1, comparative performances of controller outputs can be seen in Figure 7.8. True performance of the PBC controller over PI controller is seen more clearly in the controller output graphics in the figure 7.8. Gain of the PI controller exceeds to 1200s while the new controller is only around the 900s.

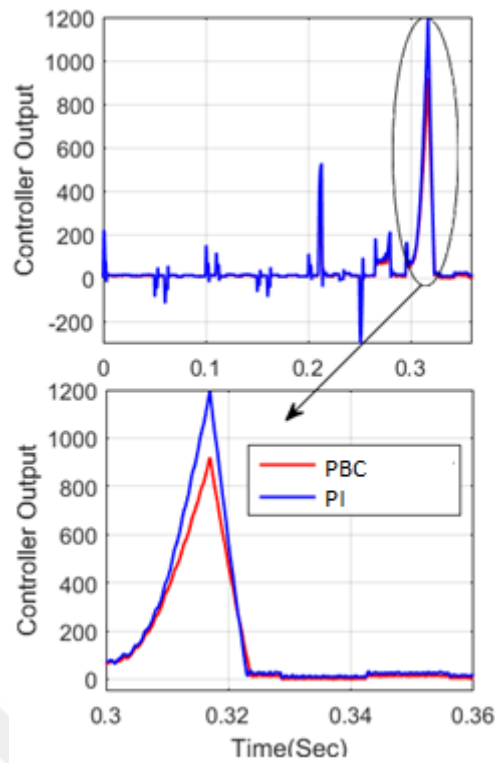


Figure 7.8 Controller outputs for case 1

Similarly, for the case 2, similar graphics are obtained. As seen in Figure 7.9, Figure 7.10 and Figure 7.11, PBC controller has the same performance with PI, even in some conditions it can show better performance over PI controller.

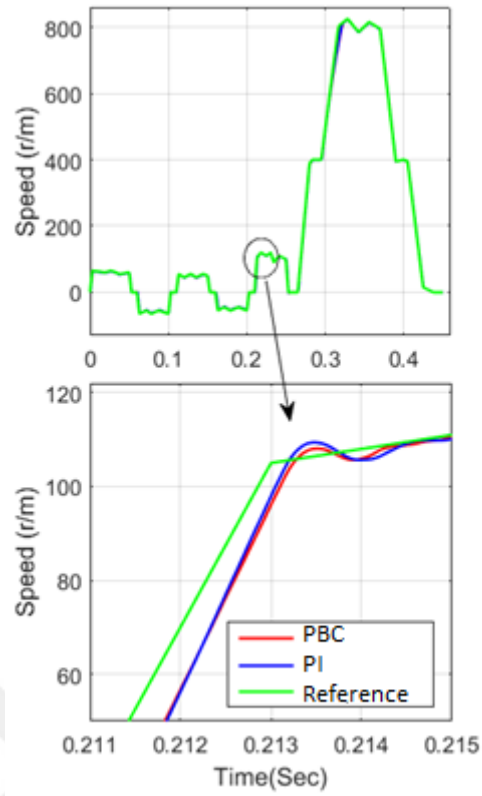


Figure 7.9 Comparative simulation results of the speed control for case 2

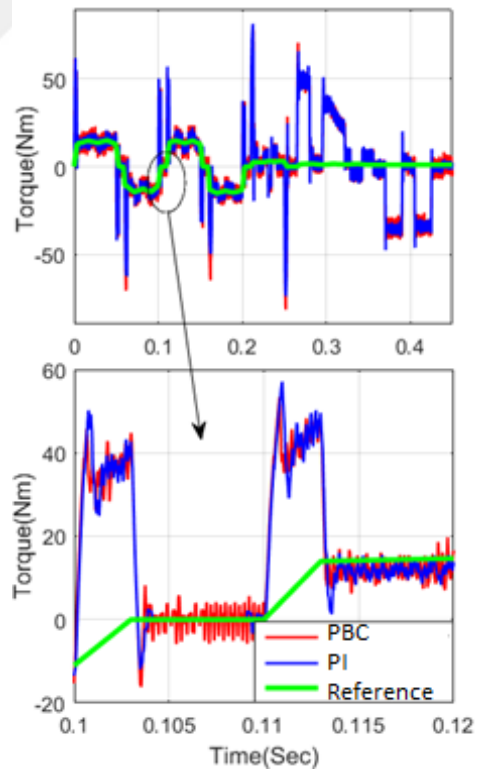


Figure 7.10 Comparative simulation results of the torque control for case 2

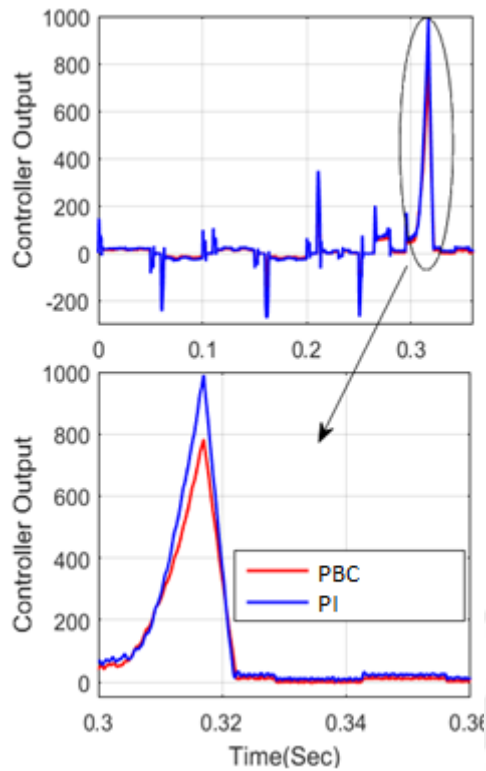


Figure 7.11 Controller outputs for case 2

In summary, the modeling of a PMSM and the simulation of the FOC scheme is achieved in MATLAB/Simulink. It can be seen in the simulation results that the proposed controller which is used as the speed and the current controllers has also a good performance. Finally, it should note that Matlab's PID tuner tool and the trial and error method are used to adjust the gain parameters of PI controllers.

8. EXPERIMENTAL RESULTS

The hardware setup of the system is conducted on the kit TMDSHVMTRPFCKIT which is integrated by TMS320F28035 DSP based on C2000 family of Texas Instrument. The software setup is modified in Code Composer Studio IDE.

The kit TMDSHVMTRPFCKIT consists of the following:

- F28035 controlCARD
- High Voltage DMC board with slot for the controlCARD
- 15V DC Power Supply
- AC power Cord, Banana Plug Cord, USB Cable
- CCS4 CD & USB Stick with Quick Start GUI and Guide

The kit is designed as to operate high voltage three phase PM and ACIM motors. Main stages of the kit is shown in Figure 8.1. The High Voltage Digital Motor Control (HVDMC) Kit enables us learning and getting experiences about driving methods of high voltage electrical machineries and using Power Factor Correction modules to increase power management of such kind of motors.

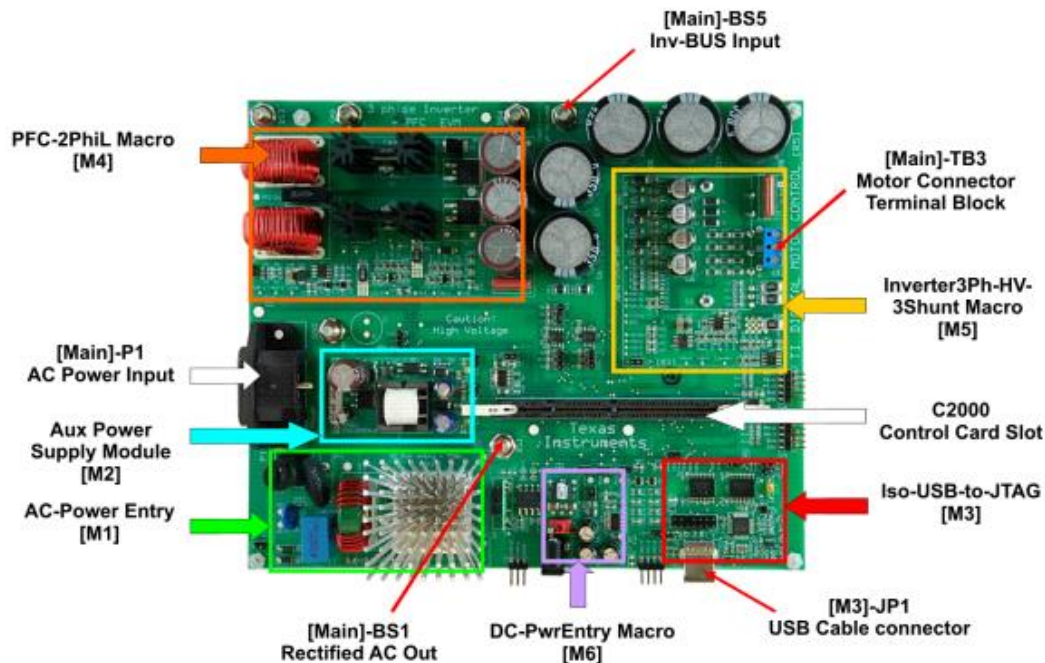


Figure 8.1 Main Stages of the Kit

As seen in Figure 8.1, The Kit has many stages that is responsible different part of a typical motor driving system. A brief introduction of each stage can be presented as:

- **3-Phase Inverter Stage** also called as Intelligent Power Module, is the main part to control our motor with determined method. This module will produce PWM outputs according to parameters that we defined in our algorithm. The rectified AC voltage is transmitted with Banana Plug Cord to the input of this module. Rated maximum DC Bus Voltage is 350 V.
- **Power Factor Correction Stage** uses some manipulation on AC input current, shape it and by reducing the leading effect of capacitances, it can regulate the DC Bus voltage for IPM inverter module to value that we desired. Therefore it can increase the efficiency of motor that will be used in the system. It can provide up to %96 efficiency for the system.
- **AC Rectifier** stage provides the necessary DC bus voltage to Inverter input by rectifying the AC main supply 110V or 220V. It is rated for 750W. It can be used both ways connecting to the Inverter input directly or provide input to the PFC stage.
- **Aux Power Supply Module** used for generate low-level voltages from rectified AC main supply voltage. Some of electronic module needs 5V-15V according to its aim. Therefore using regulation module it can reduce the max 400V DC to 5V or 15V.
- **Isolated CAN Bus** is used for communication between modules by using CAN bus protocol. These bus interfaces is isolated from high voltage stages in order not to get damaged.
- **JTAG Emulation** is used for programming and debugging processes of micro controller.
- **Four PWM DAC's** is used for observing determined variables by using oscilloscope. Observing PWM signals are most important indicator whether a module operates properly or not. Four DAC output has low pass filters in order to be able to see sinusoidal forms of PWM outputs. Isolation is an important issue for connecting oscilloscope probes to these DAC outputs.

The Digital Signal Processor (DSP) is used to perform FOC algorithm is TMS320F28035, a member of TI C2000 microcontroller family. It has high performance static CMOS Technology operating at 60MHz (16.67-ns Cycle Time), low-power supply 1.8V for DSP Core and 3.3V for the I/O buffers. The DSP controllers offer 60 MIPS of 32-bit DSP performance possible to position the edge of a PWM signal with 150 ps precision or 16 bits accuracy in a 100 KHz control loop [38-39]. Figure B.1 in the Appendix B shows a block diagram of TMS320F28035 controller.

General circuitry of experimental study is shown in Figure 8.2. There is a Power Factor Correction (PFC) stage to increase the efficiency of operation. VSI circuit composes of six Intelligent Power Modules (IPM). Both sensed and sensorless drive is enabled to perform with the kit.

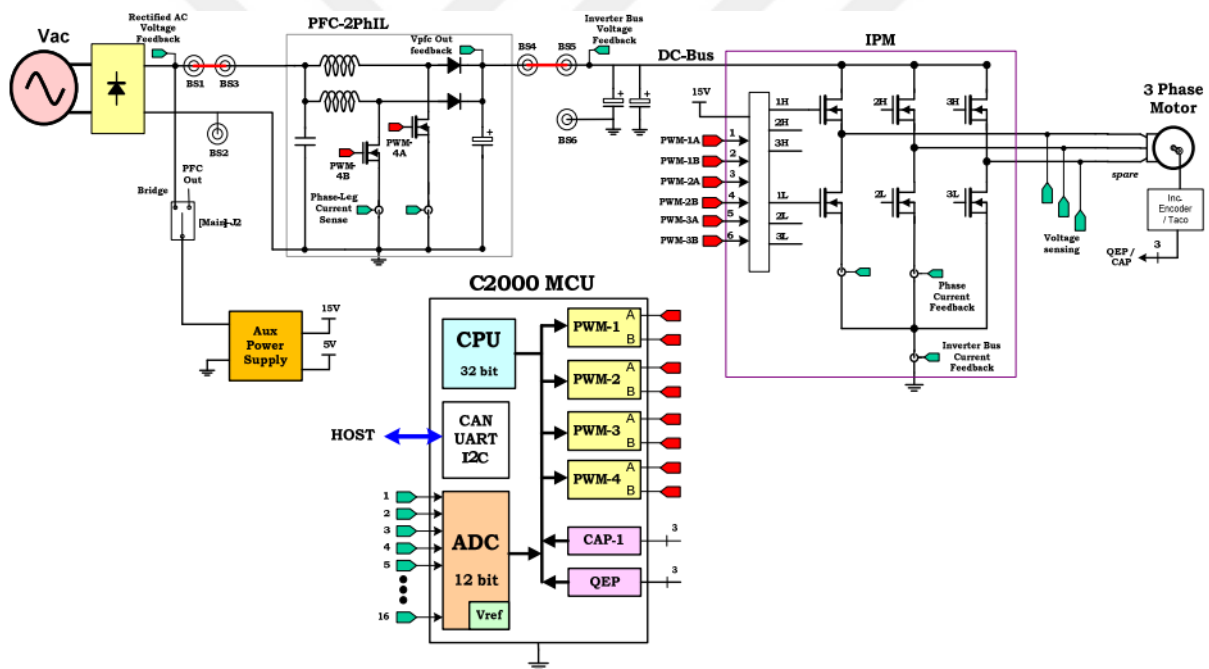


Figure 8.2 The Driver Circuit

In the study, TI's Code Composer Studio (CCS) is used to execute FOC algorithm. CCS is an Integrated Development Environment (IDE). It is used for the development of all the phases: coding the micro-controller, editor in C, linker, assembler, interface to load the program on the micro-controller as well as debugger. It also has advanced features such as real time data exchange. CCS provides a friendly environment for managing files and projects. Various library files have been provided with definitions for standardized functions and with initializations and

other standard routines for different modules. CCS comes with an editor, a compiler, an assembler and a linker [40].

The programming and the debugging processes is handled with Code Composer Studio IDE. The system consists of 6 main build levels. These build levels enables us to check module performances and each level checks different modules and adjusts the system parameters according to the results of these results. That kind of build levels called as incremental build system. Each phases of the incremental build system are designed to verify the most important software modules used in the system. As a result build levels are based on software part of the study completely. The build levels [41] are seen in Table 8.1.

Table 8.1. Build Levels of sensorless PMSM drive software

BUILDEVEL1	SVGEN_MACRO, Timers, Interrupts, PWM_MACRO is checked. The motor is not connected in this level.
BUILDEVEL2	ADC, Phase voltage calculation, Clarke-Park transformations is checked.
BUILDEVEL3	DQ axis currents values regulated by adjusted PI parameters. Speed Measurement block is tested.
BUILDEVEL4	The estimated rotor position (SMCO) and speed estimation are checked.
BUILDEVEL5	The speed regulator performed by the PI module is checked. In this level, closed loop control is conducted by the measured speed.
BUILDEVEL6	The speed regulator performed by the PI module is checked. In this level, closed loop control is conducted by the estimated speed.

Figure 8.3 shows the experimental setup. It includes a laptop used for programming and executing the system algorithm by Code Composer Studio (CCS) IDE. Texas Instruments' motor kit, HVDMMCMTRPFC which is plugged to the laptop by USB cable through the FTDI driver and measurement tools (e.g. the multimeter, the oscilloscope and the harmonic analyzer). The source code on the laptop is debugged and loaded to the memory of the DSP

TMS320F28035 control card by this cable. Controller Power comprises of the 15V, 5V and 3.3V that the board uses to power the control card and the logic and sensing circuit present on the board. This power can be sourced from Auxiliary Power supply module [M2]. Auxiliary Power supply module [M2] can generate 15V and 5V DC from rectified AC.

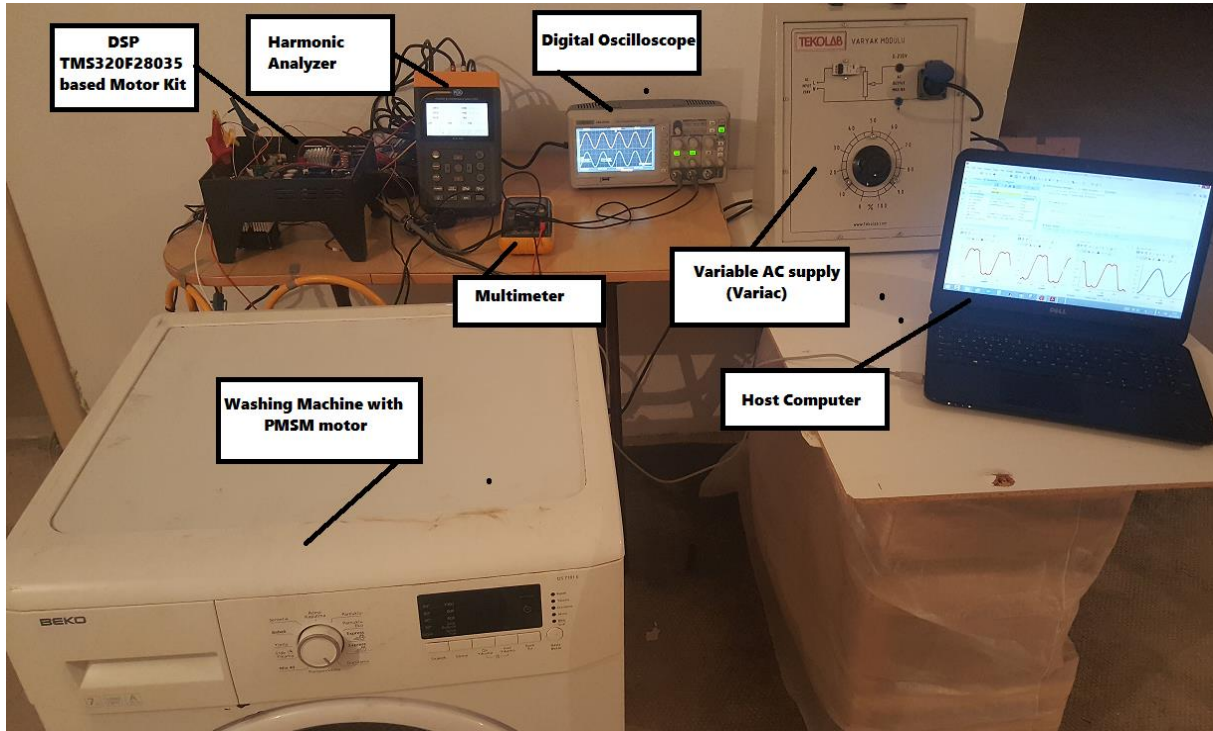


Figure 8.3 Experimental Setup

The flowchart of the proposed system is shown at Figure 8.5. The algorithm composes of two sections. The first section performs the system and module initializations, the second one executes the whole process from ADC conversion of the measured currents to SVPWM generation.

In summary, the PMSM motor is driven by the conventional VSI. The TMS320F28035 is being used to generate the gate signals using the space vector PWM technique, for intelligent power module devices in the VSI. DC-bus voltage and the stator currents of the PMSM motor (i_a and i_b) are sensed from the VSI and they are all sent to the TMS320F28035 via three separate ADC modules. The DC-bus voltage is needed to calculate three phase voltages of the PMSM motor when the switching functions are known.

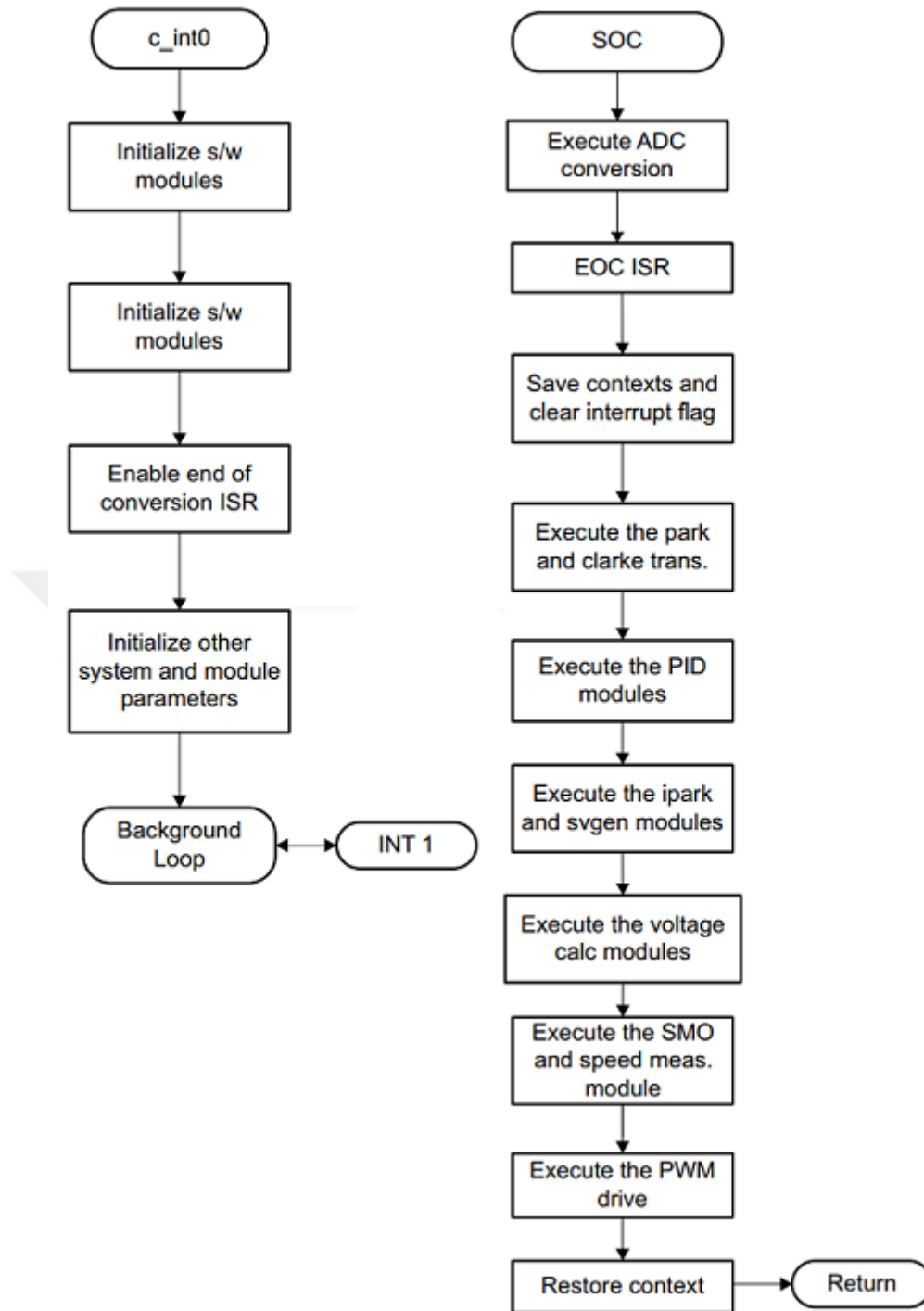


Figure 8.4 Flowchart of the proposed FOC algorithm

During the experimental study, the data and the graphics are captured to display and analysis via the debugging tool of CCS IDE and digital oscilloscope. For instance, T_a , T_b and T_c signals of SVPWM generator are shown in Figure 8.4. It should note that the same motor parameters are used as shown Table 7.1 at the chapter of simulation study.

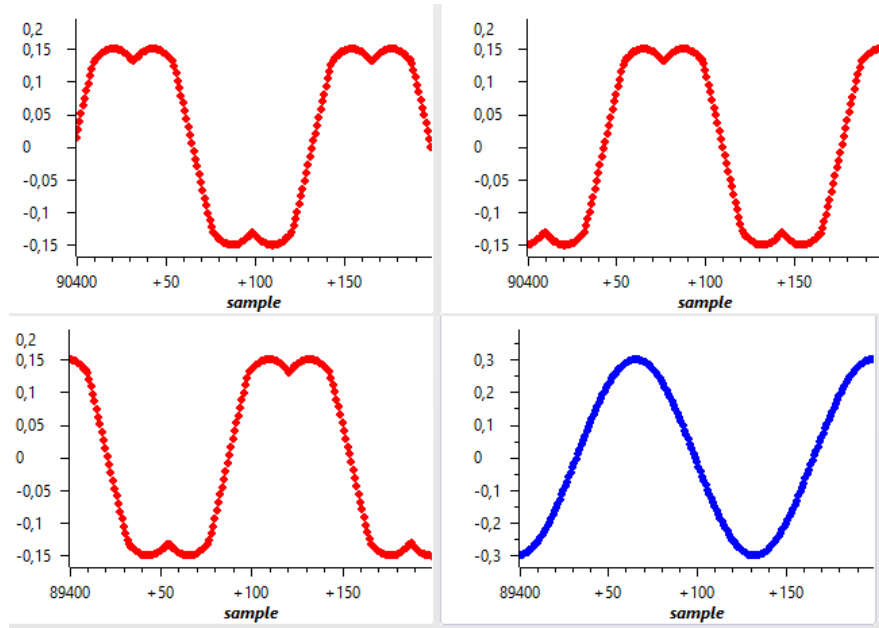


Figure 8.5 Ta, Tb and Tc and Tb-Tc signals of SVPWM Generator

The experimental study consists three types of work in terms of load torque. These are unloaded, 8kg laundry load and 800gr unbalanced load, respectively. Each sub-study is conducted up to 400RPM motor speed which is shown in Figure 8.6, in order to emulate washing cycle of the WM operation. Each condition conducted both at open loop and closed loop control.

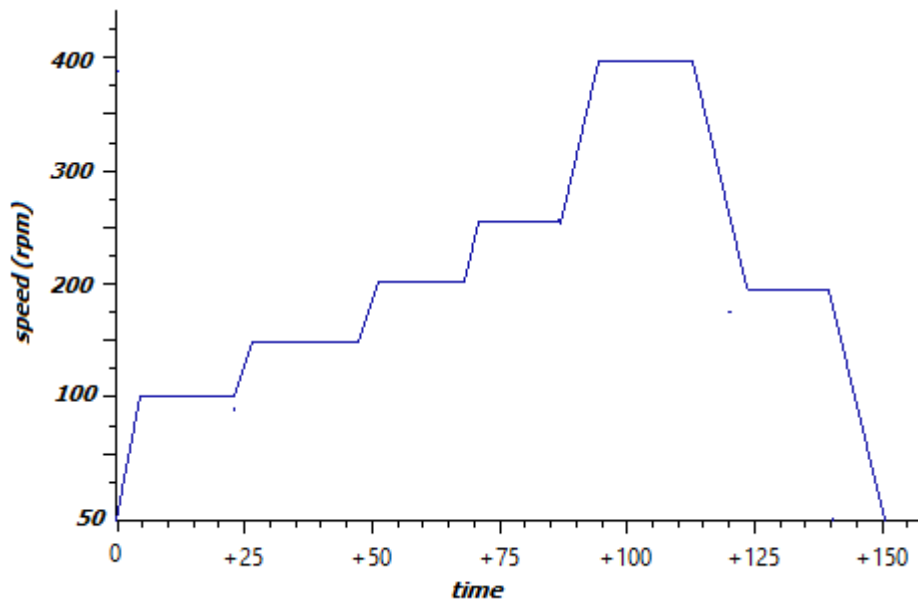


Figure 8.6 Reference Speed Graphic of PMSM motor

Figure 8.7 and 8.8 indicate open loop I_α and I_β currents in unloaded and 8kg loaded conditions, respectively.

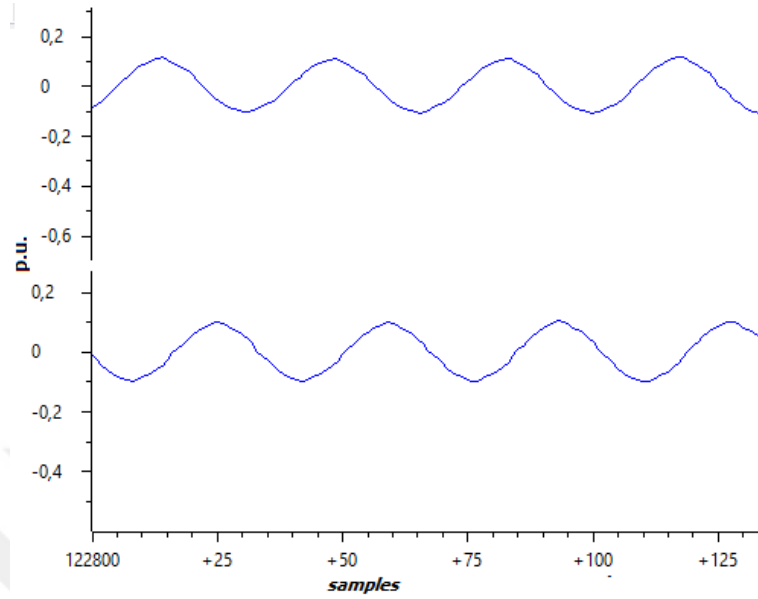


Figure 8.7 Open Loop I_α and I_β currents in unloaded drum

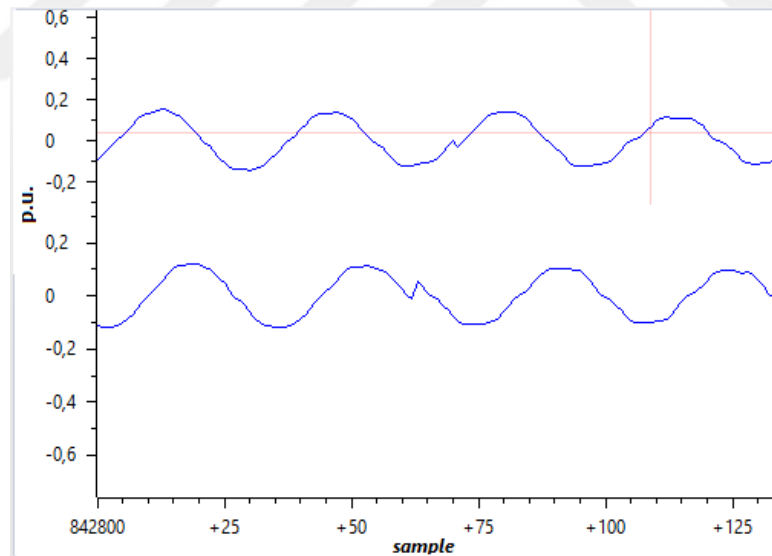


Figure 8.8 Open Loop I_α and I_β currents in 8kg loaded drum

As stated in the previously, sensorless drive is realized by SMO which is analyzed in chapter 6. The rotor flux angle is estimated by the current observer, because it equals to the electrical angle of the motor which PT and IPT require. In summary, SMO derives the BEMFs from the measured currents and compares to the estimated ones, if they are equals to each other,

it calculates the rotor position angle and the position. The estimated value of rotor position can be seen in Figure 8.9

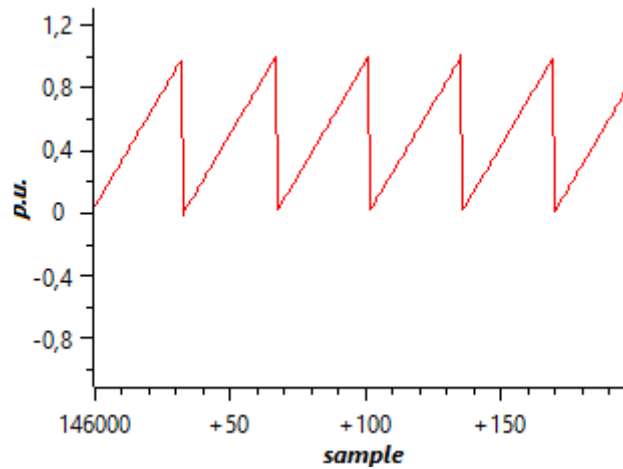


Figure 8.9 The estimated rotor angle

Note that y-axis unit, p.u. stands for “per unit” and it is organized as a special format in Code Composer Studio IDE. Actually, the rotor angle keeps rotating from 0 to 360° periodically.

Figure 8.10 and 8.11 show the same variables above when closed loop control operation are held at 400rpm motor speed, with unloaded and, 8kg loaded drum, respectively.

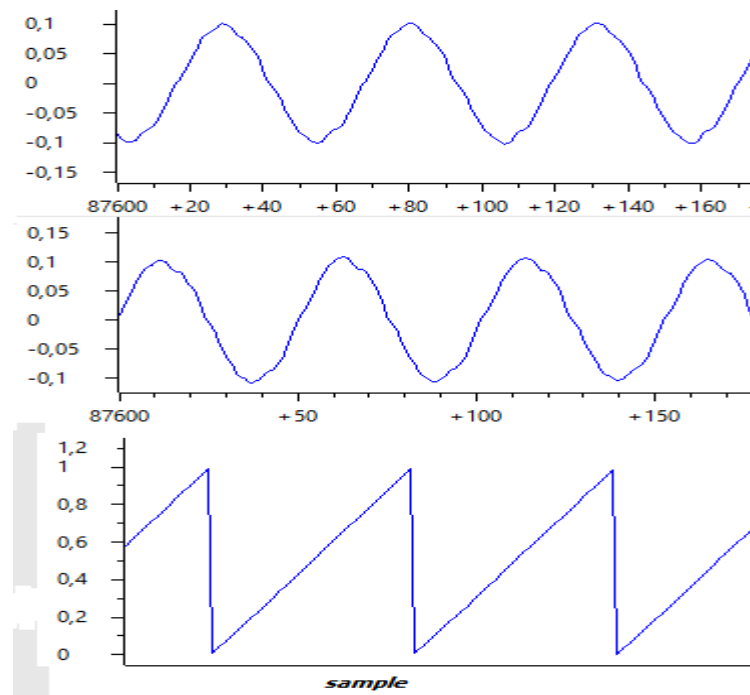


Figure 8.10 Ia, Ib currents and rotor angle at closed loop control for unloaded drum

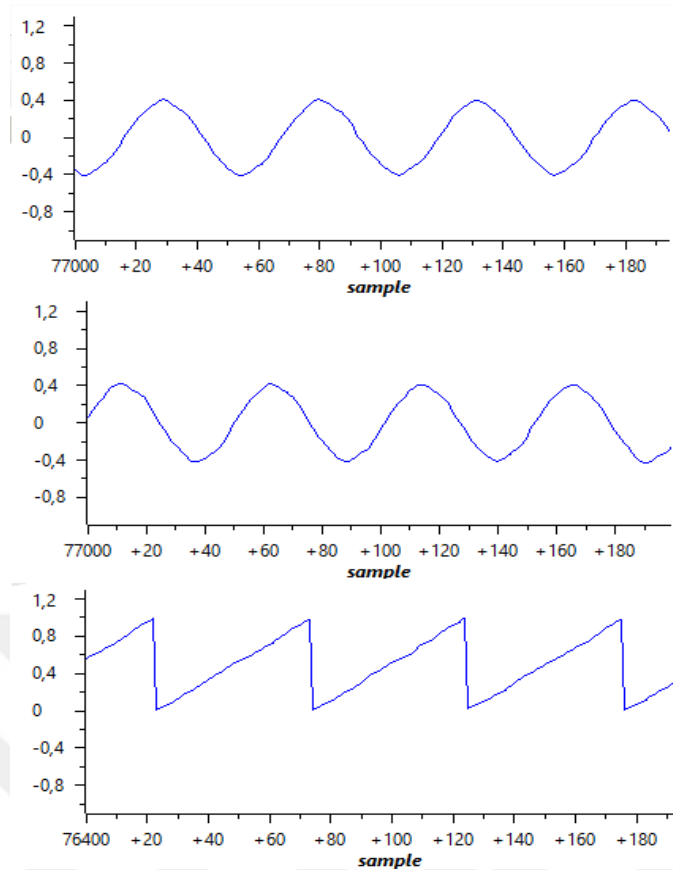


Figure 8.11 I_α , I_β currents and rotor angle at closed loop control for 8kg loaded drum

It is clear that when the drum is loaded with laundry, WM needs more torque generation, thus currents drawn from the motor increases.

Figure 8.12 shows signals from closed loop control for 800gr unbalanced load.

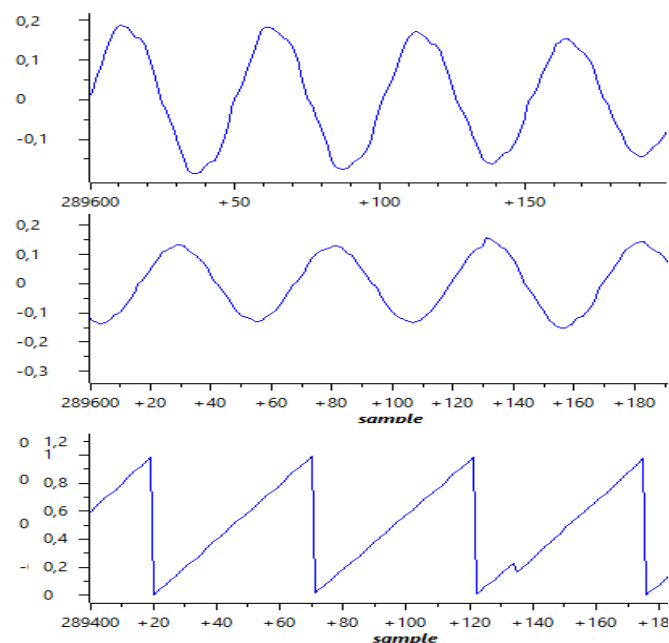


Figure 8.12 I_α , I_β currents and rotor angle at closed loop control for unbalanced drum

9. CONCLUSION

In this thesis, the modeling, the simulation and the experimental setup for a sensorless PMSM drive is studied. It is clear that designing a sensorless PMSM driver requires a variety of experience in many disciplines such as mathematic, control theory, computer algorithms and electronics. In this study a sensorless FOC driver is designed. A WM motor is chosen because of its highly dynamic behavior with unknown load changes.

In chapter 1, an overview for the thesis study is presented. In chapter 2, the operation cycles of the WM are examined with its dynamic characteristics of speed and torque before the driver design. Then a detailed information is presented for brushless permanent magnet motors generally used in WMs comparing with their advantages, disadvantages, structures, and differences. Also, the selection reasons of a PMSM are discussed in Chapter 3. In the following chapters, a dynamic model of a PMSM, Clarke and Park transformations, VSI circuit and SVPWM generator, sensorless drive techniques are presented, respectively. Lastly, the simulation and experimental results are explained using graphical sketches and tables.

The modulus of a novel control scheme called PBC is proposed for the speed and the torque control of a PMSM instead of the PI regulator. The simulation results show that the novel controller achieves a closer performance compared to the PI controller. In most cases, the proposed control scheme shows better results, particularly in speed control. Besides, the proposed control scheme is successfully used as a current regulator in the FOC. The experimental setup is implemented by a HVDMC kit based on the DSP TMS320F28035 and the experimental results are obtained using Code Composer Studio IDE of Texas Instruments.

As a future work, other estimation techniques on detection of the rotor position can be designed to evaluate the performance especially at low operation speeds.

In conclusion, the sensorless FOC drive method exhibits an effective driving performance due to its complex structure, robustness and fast dynamic response.

REFERENCES

- [1]. Lyshevski, S. E. (2000). Electromechanical Systems, Electric Machines, and Applied Mechatronics. Boca Raton, Fl: CRC Press.
- [2]. Lee, S., Lemley, T., & Keohane, G. (2009). A comparison study of the commutation methods for the three-phase permanent magnet brushless DC motor. In *Electrical Manufacturing Technical Conference 2009: Electrical Manufacturing and Coil Winding Expo* (pp. 49-55)
- [3]. Begh, Mirza & Herzog, Hans-Georg. (2018). Comparison of Field Oriented Control and Direct Torque Control. 10.13140/RG.2.2.21677.59360/1.
- [4]. Klintberg, E. (2013), Comparison of Control Approaches for Permanent Magnet Motors, Master of Science Thesis
- [5]. Pragasen Pillay and Ramu Krishnan, "Application Characteristics of Permanent Magnet Synchronous and Brushless dc Motors for Servo Drives", IEEE Trans. on Industry Apps, Vol. 27, No. 5, 1991
- [6]. Al Azze, Qasim. (2014). Field-Oriented Control of Permanent Magnet Synchronous Motors Based on DSP Controller. M.Sc. Thesis.
- [7]. Karakaş, S. (2011). Vector Control of PMSM in Washing Machine Application, M.Sc. Thesis.
- [8]. Karakaş, S., Gökasan M. (2011), An Adaptive Approach for Online Fine Tuning of Current PI Controllers in Washing Machines, Proceedings of the 2011 IEEE International Conference on Mechatronics, April 13-15, 2011, Istanbul, Turkey
- [9]. Khan, F. & Husin, Z.A. & Soomro, H. & Mazlan, M.A. & Sulaiman, E. (2016). Deterministic optimization of single phase 8S-4P field excitation flux switching motor for hybrid electric vehicle. 11. 5084-5088.
- [10]. Valchev, V.C, Yankov P.V., Marinov, A.S. (2009), PMSM/BLDC as Generators in Renewable Energy Conversion Systems, ANNUAL JOURNAL OF ELECTRONICS, 2009, ISSN 1313-1842
- [11] Pillay, P., Krishnan R.(1991), "Application Characteristics of Permanent Magnet Synchronous and Brushless dc Motors for Servo Drives", IEEE Trans. on Industry Apps, Vol. 27, No. 5, 1991

- [12]. Tang, Y., Paulides, J. J. H., Kazmin, E., & Lomonova, E. (2012). Investigation of winding topologies for permanent magnet in-wheel motors. *COMPEL: The International Journal for Computation and Mathematics in Electrical and Electronic Engineering*, 31(1), 88-107. DOI: 10.1108/03321641211184841
- [13]. Zambada, J. (2007), Application note, "Sensorless Field Oriented Control of PMSM Motors", Microchip, Inc. Chandler, Arizona www.microchip.com.
- [14]. Novak, Martin. (2012). Research Setup for Special Purpose Permanent Magnet Synchronous Machines. 10.13140/RG.2.2.24680.16649.
- [15]. Akyol, İ.E., (2016), Position Sensorless Field Oriented Control of Ipmsm Under Parameter Uncertainties, M.Sc. Thesis.
- [16]. Sivadas, S.V. (2012), Sensorless control of Permanent Magnet Synchronous Motor at low speed, M.Sc. Thesis.
- [17]. Wilamowski, B. M., & Irwin, J. D. (2011). Electronics and Motor Drives. Boca Raton, FL: CRC Press.
- [18]. Kocalmis, B.A, Sunter S., (2016), Comparison of Sinusoidal and Space Vector PWM Control Techniques for Three-Level Inverter Drives, International Journal of Electronics, Mechanical and Mechatronics Engineering. Vol.6 num.4 - 2016 (1275-1283)
- [19]. Turksoy, O., Yilmaz, U., Tan, A., Teke, A., (2017). A Comparison Study of Sinusoidal PWM and Space Vector PWM Techniques for Voltage Source Inverter. Natural and Engineering Sciences. 2. 10.28978/nesciences.330584.
- [20]. Kumar, K.V.; Michael, P.A.; John, J.P., Kumar, S.S. (2010), Simulation and comparison of SPWM and SVPWM control for three phase inverter. ARPN J. Eng. Appl. Sci. 2010, 5, 61–74
- [21]. Jose, L.A., & B.Karthikeyan, K. (2013). A Comparative Study of Sinusoidal PWM and SpaceVector PWM of a Vector Controlled BLDC Motor. International Journal of Advanced Research in Electrical, Electronics and Instrumentation Engineering Vol. 2, Issue 6
- [22]. Soni, P., Burse, K. (2012), Analysis of Voltage Source Inverters using Space Vector PWM for Induction Motor Drive, IOSR Journal of Electrical and Electronics Engineering (IOSR-JEEE) ISSN: 2278-1676 Volume 2, Issue 6, PP 14-19
- [23]. Jung J.W (2005), Project #2 Space Vector PWM inverter. Project performed at

Mechatronic Systems Laboratory, Department of Electrical and Computer Engineering, The Ohio State University, USA.

[24]. Kulkarni, S.S., Thosar A.G. (2013), Mathematical Modeling and Simulation of Permanent Magnet Synchronous Machine, International Journal of Electronics and Electrical Engineering Vol. 1, No. 2

[25]. Siwakoti Y. P., Town G.E (2013), Design of FPGA-controlled power electronics and drives using MATLAB Simulink. 571-577. 10.1109/ECCE-Asia.2013.6579155.

[26]. Tripura, P , Babu, K.Y.S , Tagore Y.R. (2011), Space Vector Pulse Width Modulation Schemes for Two-Level Voltage Source Inverter, ACEEE Int. J. on Control System and Instrumentation, Vol. 02, No. 03

[27]. Zhang, W.F, and Yu, Y.H (2007), Comparison of Three SVPWM Strategies, journal of electronic science and technology of china, vol. 5, no. 3

[28]. Mahammadsoaib, S.M., Sajid, P. M. (2015), Vector Controlled PMSM drive using SVPWM technique – A MATLAB / Simulink Implementation, 978-1-4799-7678-2/15/\$31.00 ©2015 IEEE

[29]. Munoz, D. V. (2011). Design, Simulation and Implementation of PMSM Drive System. Thesis for Master of Science & Engineering . Göteborg, Sweden.

[30]. Microsemi App Note, Field Oriented Control of Permanent Magnet Synchronous Motors User's Guide, Source: https://www.microsemi.com/document-portal/doc_view/130909-sf-foc-pmsm-hall-ug

[31]. J. Zambada and D. Deb (2011), “Sensorless field oriented control of a pmsm,” Microchip Application Note AN1078, 2011

[32]. Kivanc, O. C., & Ozturk, S. B. (2019). Low-Cost Position Sensorless Speed Control of PMSM Drive Using Four-Switch Inverter. *Energies*, 12(4), 741.

[33]. Parasiliti F., Petrella R.(2001), Sensorless Speed Control of a PM Synchronous Motor based on Sliding Mode Observer and Extended Kalman Filter, *Conference Record of the 2001 IEEE Industry Applications Conference. 36th IAS Annual Meeting (Cat. No.01CH37248)*, Chicago, IL, USA, 2001, pp. 533-540 vol.

[34]. Kung, Y.-S., Quynh, N. V., Huang, C.-C., & Huang, L.-C. (2012). Design and simulation of adaptive speed control for SMO-based sensorless PMSM drive. 2012 4th International

Conference on Intelligent and Advanced Systems (ICIAS2012).
doi:10.1109/icias.2012.6306234

[35]. Mehta, H., Joshi V., Kurulkar P. (2016), Implementation Issues of Sliding Mode Observer for Sensorless Field Oriented Control of PMSM Using TMS320F2812, IEEE Symposium on Sensorless Control for Electrical Drives (SLED).doi: 10.1109/sled.2016.7518798

[36]. Islam, A, Hossen B., Banik B., Ghosh B.C. (2017), Field Oriented Space Vector Pulse Width Modulation Control of Permanent Magnet Brushless DC Motor, IEEE Region 10 Humanitarian Technology Conference (R10-HTC) 21 - 23 Dec 2017, Dhaka, Bangladesh

[37]. Agrawal J., Bodkhe S. (2014), Functional Modeling and Simulation of Inverter Fed Permanent Magnet Synchronous Motor Drive, International Conference on Magnetism, Machines & Drives (AICERA-2014 iCMMD)

[38]. Roopa C., Sujitha S. (2018), The Implementation of Field Oriented Control for PMSM Drive Based on TMS320F28035 DSP Controller, International Journal of Applied Engineering Research ISSN 0973-4562 Volume 13, Number 6 (2018) pp. 4403-4408

[39]. Samar, A., Saedin, P., Tajudin A.I. and N. Adni (2012), "The implementation of Field Oriented Control for PMSM drive based on TMS320F2808 DSP controller," *2012 IEEE International Conference on Control System, Computing and Engineering*, Penang, 2012, pp. 612-616.

[40]. Janakiraman S. (2014), An adaptive sensorless control for maximum power point tracking in wind energy conversion system, M.Sc. Thesis, Faculty of the Department of Electrical and Computer Engineering University of Houston.

[41]. Akin B., Bhardwaj M. (2013), Sensorless Field Oriented Control of 3-Phase Permanent Magnet Synchronous Motors, Application Report, Texas Instruments. SPRABQ3–July 2013

APPENDIX A

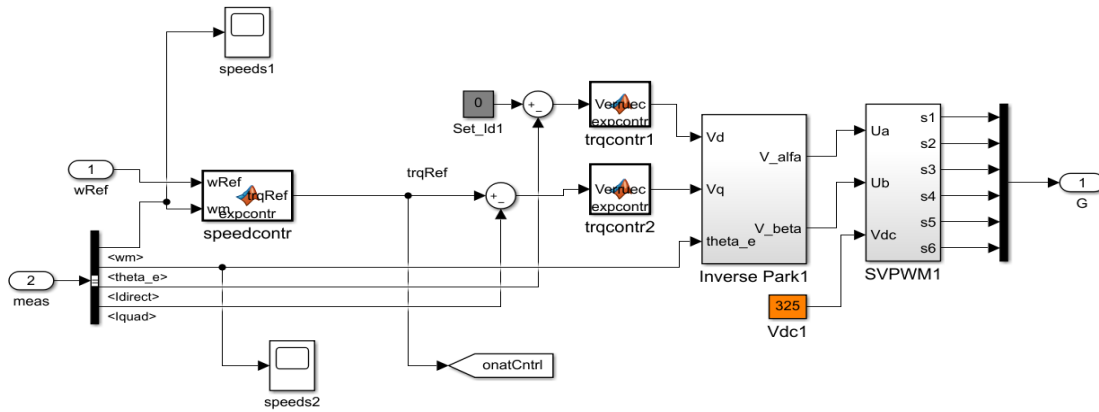


Figure A.1 PBC controller, IPT and SVPWM blocks

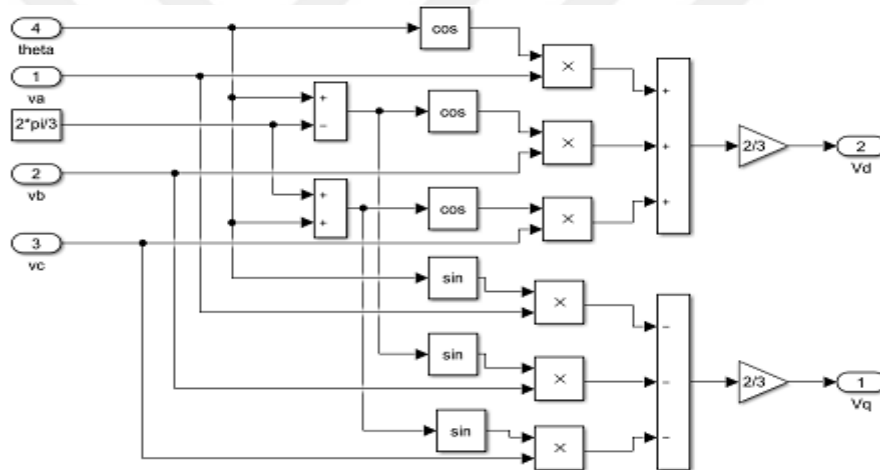


Figure A.2 abc to dq-model block in PMSM model

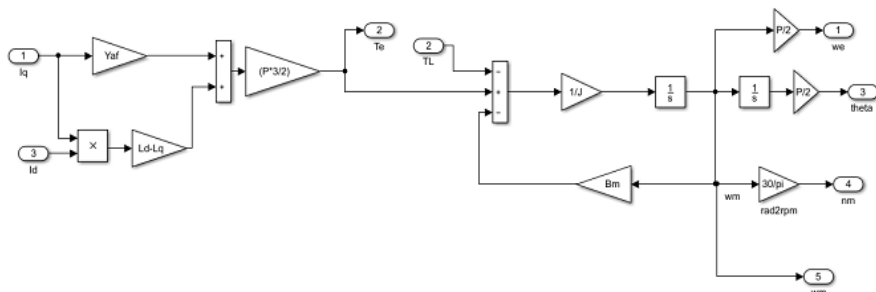


Figure A.3 Mechanical modeling block of PMSM

APPENDIX B



Figure B.1 Block diagram of DSP TMS320F28035

APPENDIX C

Sliding Mode Current Observer Macro

```

/*
=====
File name:      SMOPOS.H
=====
*/
#ifndef __SMOPOS_H__
#define __SMOPOS_H__

typedef struct {  _iq  Valpha;          // Input: Stationary alfa-axis stator
voltage          _iq  Ealpha;          // Variable: Stationary alfa-axis back EMF
                 _iq  Zalpha;          // Output: Stationary alfa-axis sliding
control
                 _iq  Gsmopos;         // Parameter: Motor dependent control gain
                 _iq  EstIalpha;       // Variable: Estimated stationary alfa-axis
stator current
                 _iq  Fsmopos;         // Parameter: Motor dependent plant matrix
                 _iq  Vbeta;           // Input: Stationary beta-axis stator voltage
                 _iq  Ebeta;           // Variable: Stationary beta-axis back EMF
                 _iq  Zbeta;           // Output: Stationary beta-axis sliding
control
                 _iq  EstIbeta;        // Variable: Estimated stationary beta-axis
stator current
                 _iq  Ialpha;          // Input: Stationary alfa-axis stator current
                 _iq  IalphaError;     // Variable: Stationary alfa-axis current
error
                 _iq  Kslide;           // Parameter: Sliding control gain
                 _iq  Ibeta;           // Input: Stationary beta-axis stator
current
                 _iq  IbetaError;      // Variable: Stationary beta-axis current
error
                 _iq  Kslf;             // Parameter: Sliding control filter gain
                 _iq  Theta;           // Output: Compensated rotor angle
                 _iq  E0;              // Parameter: 0.5
                } SMOPOS;

/*-----
Default initializer for the SMOPOS object.
-----*/
#define SMOPOS_DEFAULTS {  0,0,0,0,0,0,0,0,0,0,0, \
                          0,0,0,0,0,0,0,IQ(0.5)  \
                          }

/*-----
Prototypes for the functions in SMOPOS.C
-----*/

#define SMO_MACRO(v)

\

\

/* Sliding mode current observer */

```

```

    v.EstIalpha = _IQmpy(v.Fsmopos,v.EstIalpha) + _IQmpy(v.Gsmopos,(v.Valpha -
v.Ealpha-v.Zalpha));
    v.EstIbeta  = _IQmpy(v.Fsmopos,v.EstIbeta)  + _IQmpy(v.Gsmopos,(v.Vbeta  -
v.Ebeta  -v.Zbeta ));

    /*      \
      Current errors      */

    \
v.IalphaError = v.EstIalpha - v.Ialpha;
v.IbetaError  = v.EstIbeta  - v.Ibeta;

    \
/*      Sliding control calculator      */

/* v.Zalpha=v.IalphaError*v.Kslide/v.E0) where E0=0.5 here*/
v.Zalpha = _IQmpy(_IQsat(v.IalphaError,v.E0,-v.E0),_IQmpy2(v.Kslide));
v.Zbeta  = _IQmpy(_IQsat(v.IbetaError ,v.E0,-v.E0),_IQmpy2(v.Kslide));

    \
/*      Sliding control filter -> back EMF calculator*/
v.Ealpha = v.Ealpha + _IQmpy(v.Kslf,(v.Zalpha-v.Ealpha));
v.Ebeta  = v.Ebeta  + _IQmpy(v.Kslf,(v.Zbeta -v.Ebeta));

    \
/*      Rotor angle calculator -> Theta = atan(-Ealpha,Ebeta)      */
v.Theta = _IQatan2PU(-v.Ealpha,v.Ebeta);

#endif

```

RESUME

Fatih BAYIR

B.Sc. Computer Engineering
B.Sc. Electronics and Communication Technology
M.Sc. thesis on Sensorless PMSM Drive

Tuzla – İstanbul
bayir.fatih@gmail.com

EDUCATION

2016-Present: Marmara University Electrical and Electronics Engineering (English)
GPA 3.20 /4.00 (M. Sc.) (Thesis state)

2010-2014: Sakarya University, Computer Engineering,
GPA 2.40 /4.00 (B. Sc.)

2003-2007: Marmara University Electronics and Communication Tech. (English),
GPA 2.80 /4.00 (B. Sc.)

1999-2003: Tuzla Anadolu Meslek Lisesi (High School), Electronics

WORK EXPERIENCE

2012-Present: Electronics Teacher in MEB (National Education Ministry)

2009-2012: R&D Staff in Arçelik Washing Machine Plant.

2008-2009: Embedded System Designer in ALFA Electronics, Kartal.